JCI The Journal of Clinical Investigation

An intracellular role for ABCG1-mediated cholesterol transport in the regulated secretory pathway of mouse pancreatic β cells

Jeffrey M. Sturek, … , Raghavendra G. Mirmira, Catherine C. Hedrick

J Clin Invest. 2010;120(7):2575-2589. https://doi.org/10.1172/JCI41280.

Research Article **Metabolism**

Cholesterol is a critical component of cell membranes, and cellular cholesterol levels and distribution are tightly regulated in mammals. Recent evidence has revealed a critical role for pancreatic β cell–specific cholesterol homeostasis in insulin secretion as well as in β cell dysfunction in diabetes and the metabolic response to thiazolidinediones (TZDs), which are antidiabetic drugs. The ATP-binding cassette transporter G1 (ABCG1) has been shown to play a role in cholesterol efflux, but its role in β cells is currently unknown. In other cell types, ABCG1 expression is downregulated in diabetes and upregulated by TZDs. Here we have demonstrated an intracellular role for ABCG1 in β cells. Loss of ABCG1 expression impaired insulin secretion both in vivo and in vitro, but it had no effect on cellular cholesterol content or efflux. Subcellular localization studies showed the bulk of ABCG1 protein to be present in insulin granules. Loss of ABCG1 led to altered granule morphology and reduced granule cholesterol levels. Administration of exogenous cholesterol restored granule morphology and cholesterol content and rescued insulin secretion in ABCG1-deficient islets. These findings suggest that ABCG1 acts primarily to regulate subcellular cholesterol distribution in mouse β cells. Furthermore, islet ABCG1 expression was reduced in diabetic mice and restored by TZDs, implicating a role for regulation of islet ABCG1 expression in diabetes pathogenesis and treatment.

An intracellular role for ABCG1-mediated cholesterol transport in the regulated secretory pathway of mouse pancreatic β cells

Jeffrey M. Sturek,[1] J. David Castle,[2] Anthony P. Trace,[3] Laura C. Page,[4] Anna M. Castle,[2] Carmella Evans-Molina,[5] John S. Parks,[6] Raghavendra G. Mirmira,[5,7] and Catherine C. Hedrick[8]

[1]Department of Pharmacology, [2]Department of Cell Biology, [3]Department of Biochemistry and Molecular Genetics, University of Virginia School of Medicine, Charlottesville, Virginia, USA. [4]School of Medicine, University of Virginia, Charlottesville, Virginia, USA. [5]Department of Medicine, Herman B. Wells Center for Pediatric Research, Indiana University School of Medicine, Indianapolis, Indiana, USA. [6]Department of Pathology, Section on Lipid Sciences, Wake Forest University School of Medicine, Winston-Salem, North Carolina, USA. [7]Department of Pediatrics and Department of Cellular and Integrative Physiology, Herman B. Wells Center for Pediatric Research, Indiana University School of Medicine, Indianapolis, Indiana, USA. [8]La Jolla Institute for Allergy and Immunology, La Jolla, California, USA.

Cholesterol is a critical component of cell membranes, and cellular cholesterol levels and distribution are tightly regulated in mammals. Recent evidence has revealed a critical role for pancreatic β cell–specific cholesterol homeostasis in insulin secretion as well as in β cell dysfunction in diabetes and the metabolic response to thiazolidinediones (TZDs), which are antidiabetic drugs. The ATP-binding cassette transporter G1 (ABCG1) has been shown to play a role in cholesterol efflux, but its role in β cells is currently unknown. In other cell types, ABCG1 expression is downregulated in diabetes and upregulated by TZDs. Here we have demonstrated an intracellular role for ABCG1 in β cells. Loss of ABCG1 expression impaired insulin secretion both in vivo and in vitro, but it had no effect on cellular cholesterol content or efflux. Subcellular localization studies showed the bulk of ABCG1 protein to be present in insulin granules. Loss of ABCG1 led to altered granule morphology and reduced granule cholesterol levels. Administration of exogenous cholesterol restored granule morphology and cholesterol content and rescued insulin secretion in ABCG1-deficient islets. These findings suggest that ABCG1 acts primarily to regulate subcellular cholesterol distribution in mouse β cells. Furthermore, islet ABCG1 expression was reduced in diabetic mice and restored by TZDs, implicating a role for regulation of islet ABCG1 expression in diabetes pathogenesis and treatment.

Introduction

Cholesterol is an essential component of cell membranes, and cellular cholesterol homeostasis is a tightly regulated process (1). Membrane cholesterol content and distribution must be maintained at finely tuned levels, and conditions of both cholesterol overload and cholesterol deficiency can result in cellular dysfunction and disease. One hallmark of type 2 diabetes is impaired insulin secretion with progressive pancreatic β cell dysfunction in the face of peripheral insulin resistance (2). Many potential pathways for β cell dysfunction in diabetes have been proposed (3), but the precise mechanisms remain elusive. Associations between dyslipidemia and diabetes have long been recognized (4), but the reasons for this relationship have not been clear. Recent work has demonstrated an important role for β cell–specific cholesterol homeostasis in β cell function (5). Inactivation of the ABC transporter A1 (ABCA1) in β cells led to islet cholesterol accumulation and markedly impaired insulin secretion (6). Importantly, loss of β cell ABCA1 abrogated the whole-animal metabolic response to the antidiabetic thiazolidinedione (TZD) rosiglitazone, implicating an important role for β cell cholesterol homeostasis in the response to clinical therapy. Studies in mouse models of diabetes and dyslipidemia have also shown increased total islet cholesterol content and demonstrated a role for this increased cholesterol in the impairment of glucose sensing and insulin secretion (7). In addition to studies of islet cholesterol accumulation, studies of cholesterol depletion, using either the cholesterol scavenger methyl-β-cyclodextrin (MβCD) (8) or an inhibitor of endogenous cholesterol synthesis (9), have demonstrated a requirement for cholesterol in regulated insulin secretion.

The ABC transporter G1 (ABCG1) has been demonstrated to promote cholesterol efflux to HDL (10), but the mechanism by which ABCG1 mediates cholesterol efflux is not well understood. In contrast to ABCA1, which specifically couples cholesterol efflux to the acceptor ApoA1 (11, 12), the efflux activity of ABCG1 is relatively nonspecific, as it can promote efflux not only to HDL but also to LDL and to cyclodextrin (10). Additionally, though ABCG1 can traffic to the plasma membrane, several studies in different cell types have shown the bulk of it to be intracellular (13, 14). Whether ABCG1 is mainly mobilized to the cell surface to support cholesterol efflux (14) or regulates intracellular cholesterol distribution remains unclear.

Studies from our laboratory have shown decreased expression of ABCG1 in macrophages from diabetic mice (15) and humans (16), and this effect could be recapitulated by chronic culture in high glucose in vitro (15). Furthermore, ABCG1 is transcriptionally upregulated by the nuclear receptor PPARγ (17, 18), which is the pharmacologic target of TZDs. Despite these findings and an emerging role for cellular cholesterol homeostasis in β cell function,

Conflict of interest: The authors have declared that no conflict of interest exists.
Citation for this article: *J Clin Invest.* 2010;120(7):2575–2589. doi:10.1172/JCI41280.

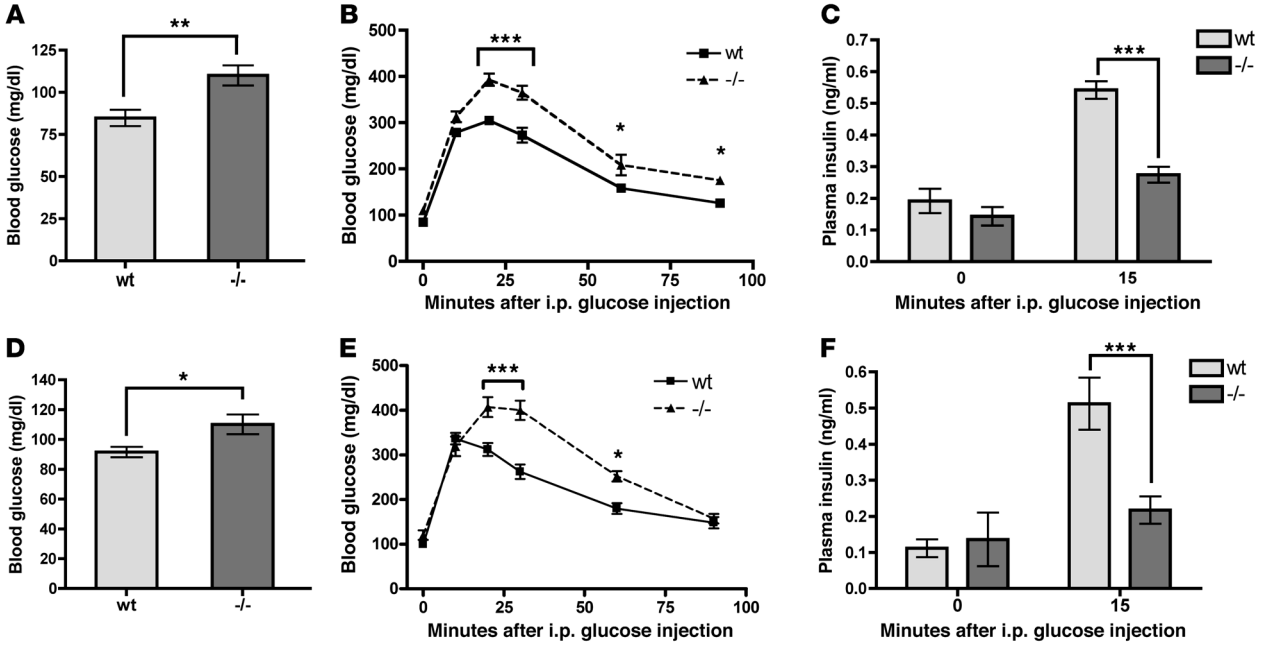

Figure 1
Loss of ABCG1 leads to impaired glucose tolerance and insulin secretion in vivo. (**A**–**C**) Data from male WT and *Abcg1*$^{-/-}$ mice, age 3 months. (**D**–**F**) Data from female WT and *Abcg1*$^{-/-}$ mice, age 3 months. (**A**, **D**) Mice were fasted overnight, and blood glucose levels were measured (n = 8 for males, 12 for females). (**B**, **E**) Fasted mice were injected with glucose i.p., and blood glucose levels were monitored over 90 minutes (n = 8 for males, 6 for females). (**C**, **F**) Plasma insulin levels were measured at fasting, and 15 minutes after i.p. glucose injection (n = 12–14 for males, 5–13 for females). Data are presented as mean ± SEM. *P < 0.05; **P < 0.01; ***P < 0.001.

no study to date, to our knowledge, has investigated ABCG1's role in this context. Here, we establish that ABCG1 supports insulin secretion, but more importantly, we highlight that this involves what we believe to be a novel intracellular action. ABCG1 largely localizes to insulin granules and appears to promote organelle cholesterol retention that is required for the function of the regulated secretory pathway. Furthermore, we show that islet ABCG1 expression is downregulated in disease and upregulated by TZD treatment, implicating a role for the maintenance of intracellular cholesterol distribution by ABCG1 in diabetes pathogenesis and treatment.

Results

Abcg1$^{-/-}$ *mice have impaired glucose tolerance and insulin secretion with normal insulin sensitivity*. To investigate the role of ABCG1 in pancreatic β cell function, we first examined the expression pattern of *ABCG1* mRNA and protein in pancreatic tissues. Conventional RT-PCR on isolated C57BL/6 mouse islets and 2 mouse pancreatic β cell lines, βTC-3 and MIN6, showed high levels of *ABCG1* mRNA in these tissues (Supplemental Figure 1A; supplemental material available online with this article; doi:10.1172/JCI41280DS1). This expression was enriched compared with whole pancreas and was comparable to expression levels in whole brain, where ABCG1 is highly expressed (13). Western blotting confirmed protein expression and validated both loss of the ABCG1 band by siRNA-mediated knockdown or gene ablation and induction by liver x receptor (LXR) agonist (Supplemental Figure 1B).

Given the enrichment of ABCG1 expression in pancreatic β cells, we next examined the role of ABCG1 in whole-animal glucose metabolism. Fasting blood glucose values of 10- to 12-week-old male *Abcg1*$^{-/-}$ mice (19) on a C57BL/6 background (backcrossed at least 10 generations) were slightly but significantly elevated as compared with WT (Figure 1A). Intraperitoneal glucose and insulin tolerance testing revealed impaired glucose clearance beginning at 20 minutes (Figure 1B) with normal insulin sensitivity (Supplemental Figure 2). This was accompanied by a 50% reduction in plasma insulin at 15 minutes after i.p. glucose injection (Figure 1C), consistent with a primary β cell defect. Experiments with female mice yielded similar results (Figure 1, D–F), suggesting that these metabolic effects are not gender specific.

Isolated ABCG1-deficient islets have reduced GSIS with normal glucose sensing. Our in vivo findings in the *Abcg1*$^{-/-}$ mice led us to hypothesize that ABCG1 may play an important role in pancreatic β cell function. Immunohistochemical analysis of pancreata from WT and *Abcg1*$^{-/-}$ mice showed no change in total insulin staining (Figure 2, A and B), suggesting that loss of ABCG1 does not alter β cell mass. Instead, isolated islets from *Abcg1*$^{-/-}$ mice showed reduced glucose-stimulated insulin secretion (GSIS) as compared with WT (Figure 2C). The decrease observed in *Abcg1*$^{-/-}$ islets was not accounted for by increased basal secretion, in agreement with the unaffected fasting plasma insulin levels (Figure 1, C and F). Together, these results imply that islet-specific ABCG1 plays a role in regulated insulin secretion.

Insulin secretion is initiated by glucose uptake through the β cell's constitutive GLUT2 transporter, and the ensuing glucose phosphorylation, oxidative metabolism, and ATP generation lead to K_{ATP} channel closure. The resulting membrane depolarization and calcium (Ca^{2+}) influx through voltage-gated Ca^{2+} channels trigger soluble NSF attachment protein receptor (SNARE) complex–mediated exocytosis of insulin granules (20). To begin to dissect the mechanism of impaired insulin secretion in *Abcg1*$^{-/-}$ islets, we assessed glucose sensing as judged by changes in intracellular calci-

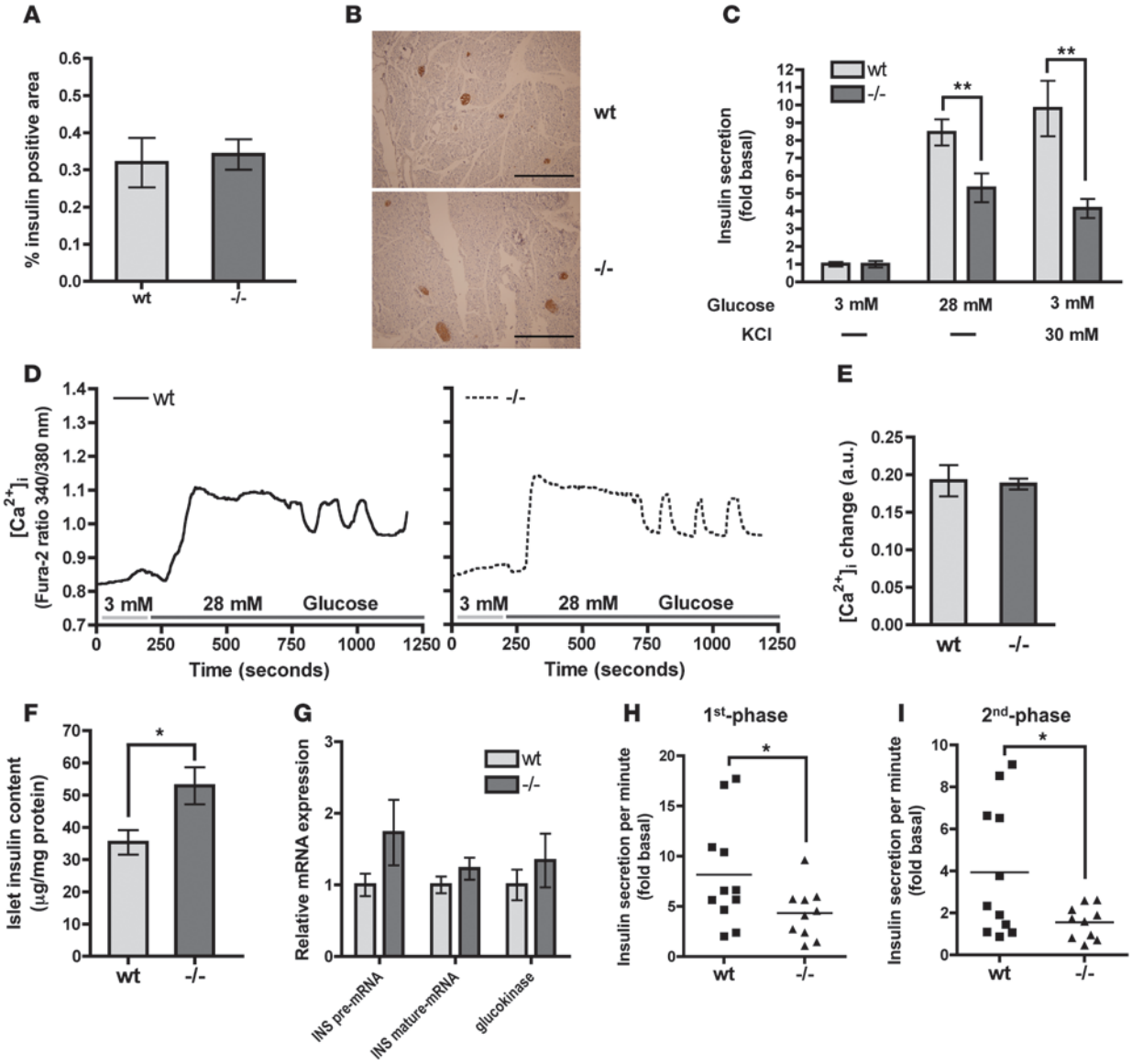

Figure 2

ABCG1-deficient islets have impaired insulin secretion in vitro. (**A** and **B**) Pancreata from WT and *Abcg1*$^{-/-}$ mice were fixed, sectioned, and immunostained for insulin, and the total β cell area as determined by insulin-positive staining was quantified (n = 8). Scale bars: 500 μm. (**C**) Islets were isolated from WT and *Abcg1*$^{-/-}$ mice, and glucose- and potassium-induced insulin secretions were measured in vitro (n = 9–22, groups of 50 islets). (**D** and **E**) Isolated islets were loaded with the calcium dye fura-2, and $[Ca^{2+}]_i$ changes in response to glucose perifusion were measured over time. (**D**) Representative curves of $[Ca^{2+}]_i$ oscillations from WT and *Abcg1*$^{-/-}$ islets. (**E**) Average net increases in $[Ca^{2+}]_i$ from basal to glucose-stimulated (n = 33–43 islets). (**F**) Insulin content from isolated islets (n = 10). (**G**) mRNA was harvested from isolated islets, and qRT-PCR was performed for transcript levels of the unprocessed insulin pre-mRNA, the mature processed insulin mRNA (transcripts for both insulin genes I and II were captured), and the regulatory enzyme glucokinase (n = 5–10). (**H** and **I**) First- and second-phase insulin secretion from WT and *Abcg1*$^{-/-}$ islets was measured by successive static incubations (first phase, 5 minutes in 30 mM KCl; second phase, 10 minutes in 28 mM glucose) (n = 10–11, groups of 50 islets). Data are presented as mean ± SEM. *P < 0.05; **P < 0.01.

um concentration ($[Ca^{2+}]_i$) measured by the ratiometric calcium dye fura-2. Raising the extracellular glucose concentration from 3 mM to 28 mM produced similar net increases in $[Ca^{2+}]_i$ in WT and *Abcg1*$^{-/-}$ islets (Figure 2, D and E), and the initial response in both cases was followed by characteristic $[Ca^{2+}]_i$ oscillations (21, 22). These data suggest that loss of ABCG1 does not impair glucose sensing. Furthermore, stimulation by direct depolarization with 30 mM KCl revealed an insulin secretory defect similar to that observed in response to glucose (Figure 2C), indicative of a defect distal to K_{ATP} channel closure. Interestingly, *Abcg1*$^{-/-}$ islets exhibited increased insulin content (Figure 2F), consistent with a slight but nonsignificant increase in pancreatic insulin content (WT = 169 ± 13 μg/g tissue; *Abcg1*$^{-/-}$ = 181 ± 9 μg/g tissue, n = 6 each) as well as normal mRNA levels of the processed mature-insulin transcript, the unprocessed preinsulin transcript, and the regulatory enzyme glucokinase (Figure 2G). These findings indicate that *Abcg1*$^{-/-}$ β cells sense

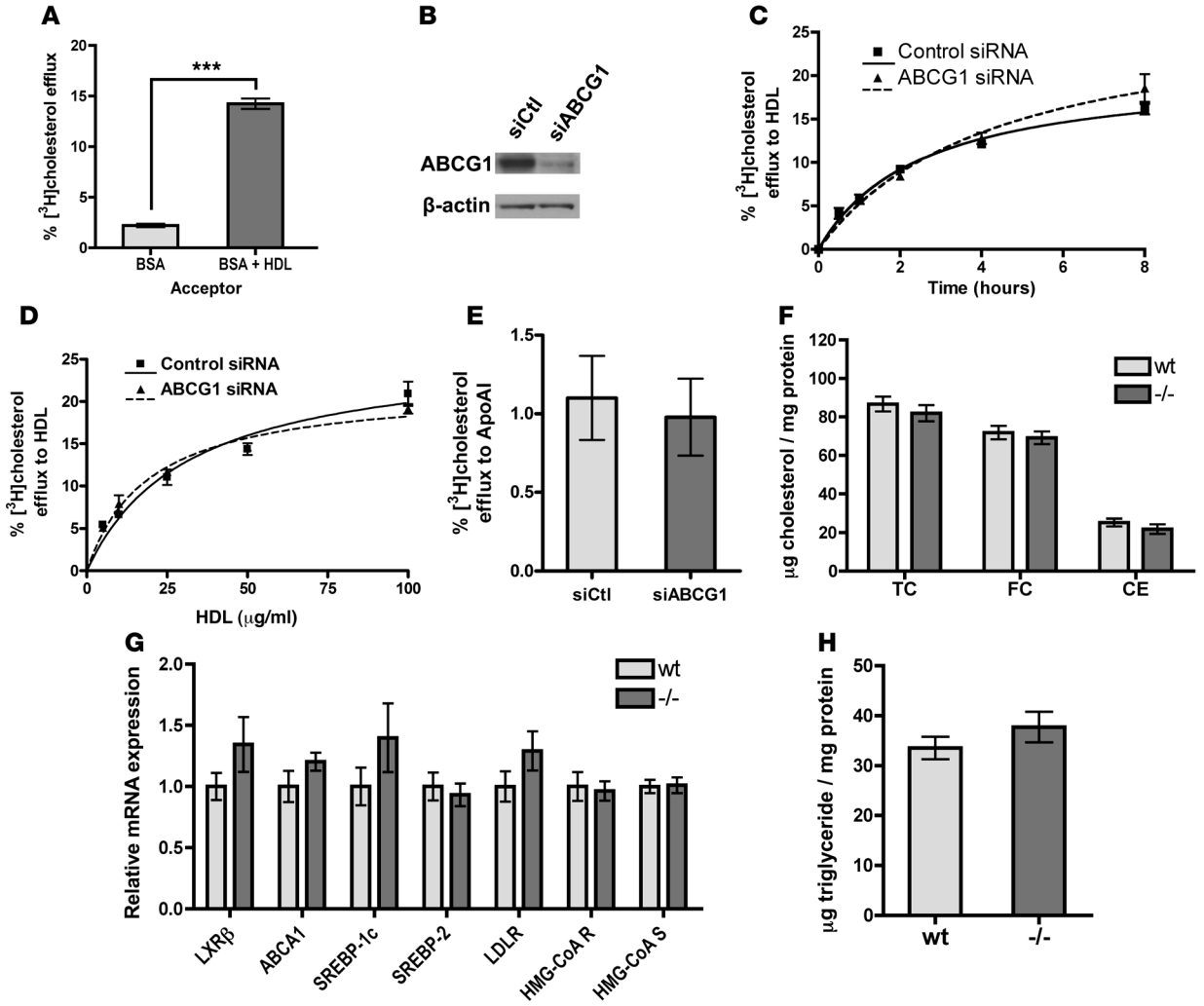

Figure 3

ABCG1 deficiency does not alter total β cell cholesterol content or efflux. (**A**) MIN6 cells were labeled with [^{3}H]cholesterol overnight, and [^{3}H]cholesterol efflux to extracellular acceptors over 4 hours was measured (n = 6). (**B**) Western blotting showing siRNA-mediated knockdown of ABCG1 in MIN6 cells (approximately 90% by densitometry). (**C**, **D**) MIN6 cells were treated with siRNA as in **B** and a time-course (**C**) and dose-response curve (**D**) of HDL-mediated [^{3}H]cholesterol efflux was measured (n = 4; representative of 3 independent experiments). (**E**) ApoAI-mediated cholesterol efflux was measured in MIN6 cells treated with ABCG1 siRNA. (**F**) Islets were isolated from WT and *Abcg1*$^{-/-}$ mice and total cholesterol (TC), free-cholesterol (FC), and cholesterol-ester (CE) content were measured by gas chromatography (150 islets per sample, n = 14 mice per group). (**G**) qRT-PCR was performed on isolated islets for cholesterol- (SREBP-2, LDLR, HMG-CoA R, HMG-CoA S) and oxysterol-regulated (ABCA1, SREBP-1c) mRNA (n = 5–10 mice per genotype). (**H**) Triglyceride content was measured in isolated islets from WT and *Abcg1*$^{-/-}$ mice (200 islets per sample, n = 8 mice per genotype). LDLR, LDL receptor; HMG-CoA R, HMG-CoA reductase; HMG-CoA S, HMG-CoA synthase. Data are presented as mean ± SEM. ***P < 0.001.

glucose and synthesize insulin normally and suggest that the defect in secretion is at the level of insulin release.

Insulin secretion typically occurs in 2 kinetic phases; the first is mediated by morphologically docked and primed granules, and the second by mobilization and release from a reserve pool (20). To better understand the defect in granule exocytosis in ABCG1-deficient islets, we approximated first- and second-phase insulin secretion using static incubations, similar to previous studies (23). Both phases were impaired in *Abcg1*$^{-/-}$ islets (Figure 2, H and I). In aggregate, our in vitro studies of insulin secretion indicate that in the absence of ABCG1, there is a change in insulin granule releasability that impairs stimulus-secretion coupling.

Loss of ABCG1 does not alter β cell cholesterol content or efflux. Given the established role for ABCG1 in cholesterol efflux to HDL, we hypothesized that the secretory defect in *Abcg1*$^{-/-}$ islets may be due to β cell cholesterol accumulation secondary to impaired cholesterol efflux. Therefore, we assessed the role of ABCG1 in cellular cholesterol homeostasis using both ABCG1-directed siRNA in the MIN6 β cell line and isolated islets from *Abcg1*$^{-/-}$ mice. MIN6 cells showed robust efflux of cholesterol to HDL, similar to levels observed in other cell types (Figure 3A) (10). However, siRNA knockdown of ABCG1 protein levels by 90% (Figure 3B) had no effect on HDL-mediated cholesterol efflux at any time point or HDL concentration tested (Figure 3, C and D) and no effect on

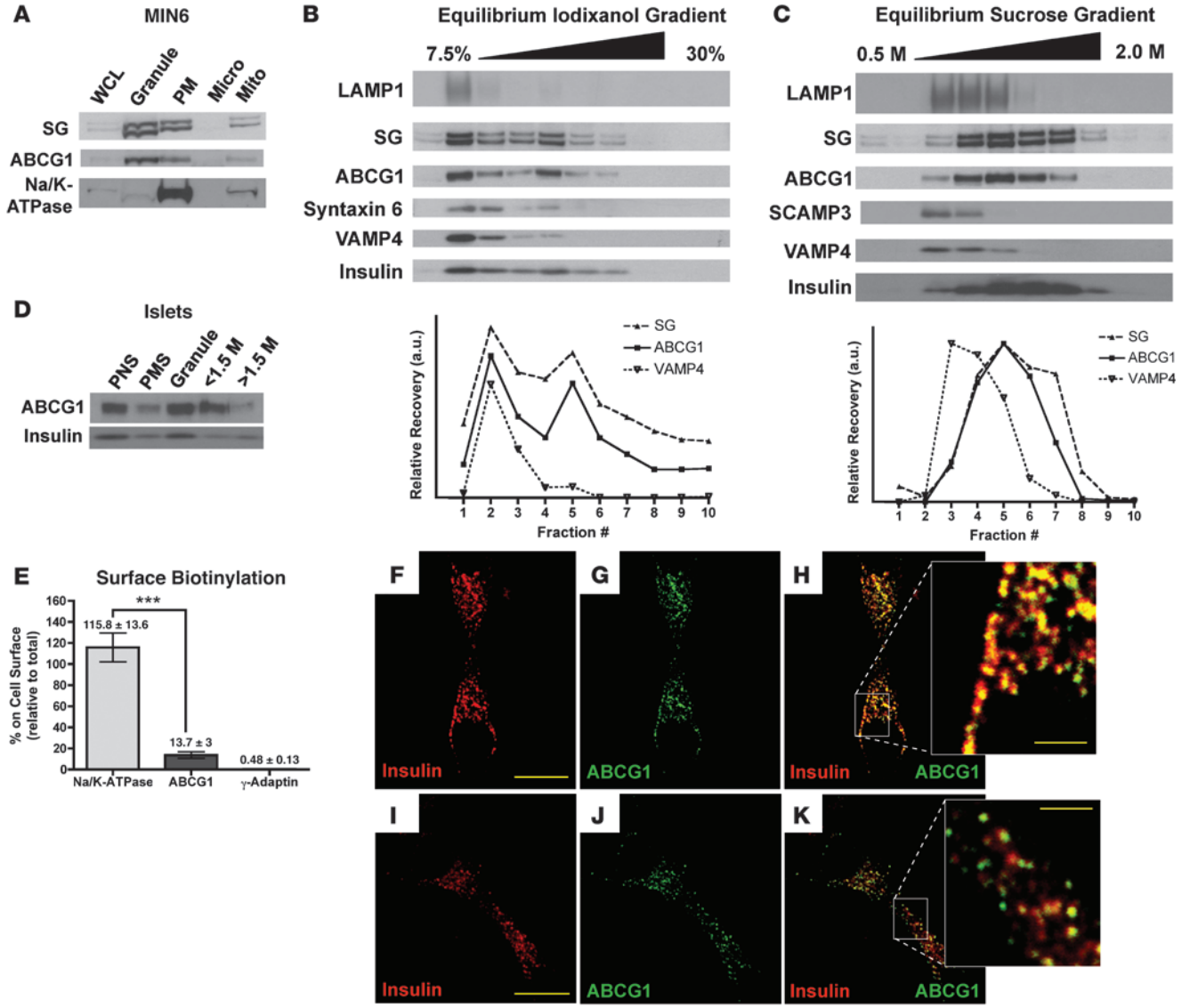

Figure 4

ABCG1 localizes substantially to the regulated secretory pathway. (**A**) MIN6 cells were homogenized, organelles were separated by differential centrifugation, and fractions were blotted for ABCG1, the granule marker secretogranin (SG), and the plasma membrane (PM) marker Na/K-ATPase. Mito, mitochondria. (**B**, **C**) The granule fraction from **A** was subfractionated on 2 different continuous density gradients, iodixanol (**B**), and sucrose (**C**), and blotted for ABCG1; SG and insulin (granules); syntaxin 6 and VAMP4 (immature granules); SCAMP3 (TGN and endosomes); and LAMP1 (late endosome/lysosome). (**D**) Approximately 1500 mouse islets were homogenized and fractionated, with subfractionation of the granules on a discontinuous sucrose gradient, collected in 2 fractions: that which floated above 1.5 M sucrose (<1.5 M) and that which pelleted through 1.5 M sucrose (>1.5 M). PNS, post-nuclear supernatant; PMS, post-mitochondrial supernatant. (**E**) MIN6 cells were surface labeled with biotin and the relative amount of ABCG1 on the cell surface was quantified by Western blotting. The plasma membrane marker Na/K-ATPase and the cytoplasmic protein γ-adaptin are shown as positive and negative controls. Numbers over bars represent mean ± SEM (n = 6, 3 independent experiments). (**F**–**K**) MIN6 cells were costained for insulin (red) and ABCG1 (green) and imaged by confocal microscopy. Scale bars: 10 μm; 2 μm (insets). Panels **F**–**H** and **I**–**K** are from 2 different fields. ***P < 0.001.

ApoAI-mediated cholesterol efflux (Figure 3E). Additionally, WT and *Abcg1*$^{-/-}$ islets showed no difference in total-, free-, or esterified-cholesterol content (Figure 3F). Furthermore, transcriptional profiling of islets from WT and *Abcg1*$^{-/-}$ mice showed no significant change in oxysterol-regulated (ABCA1 and SREBP-1c) or cholesterol-regulated (SREBP-2, LDL receptor, HMG-CoA reductase, and HMG-CoA synthase) mRNA expression (Figure 3G). Finally, there is some evidence that in adipocytes, ABCG1 may play a role in triglyceride storage (24). Given the established role of free fatty acids and triglycerides in β cell function, we also measured triglyceride content in isolated islets from WT and *Abcg1*$^{-/-}$ mice. Results from these studies showed no difference between groups (Figure 3H). Importantly, *Abcg1*$^{-/-}$ mice had normal plasma lipoprotein profiles (Supplemental Figure 3), so the *Abcg1*$^{-/-}$ β cells were not exposed to different cholesterol-loading conditions in vivo prior to islet isolation. Together, these findings suggest that, at least under basal con-

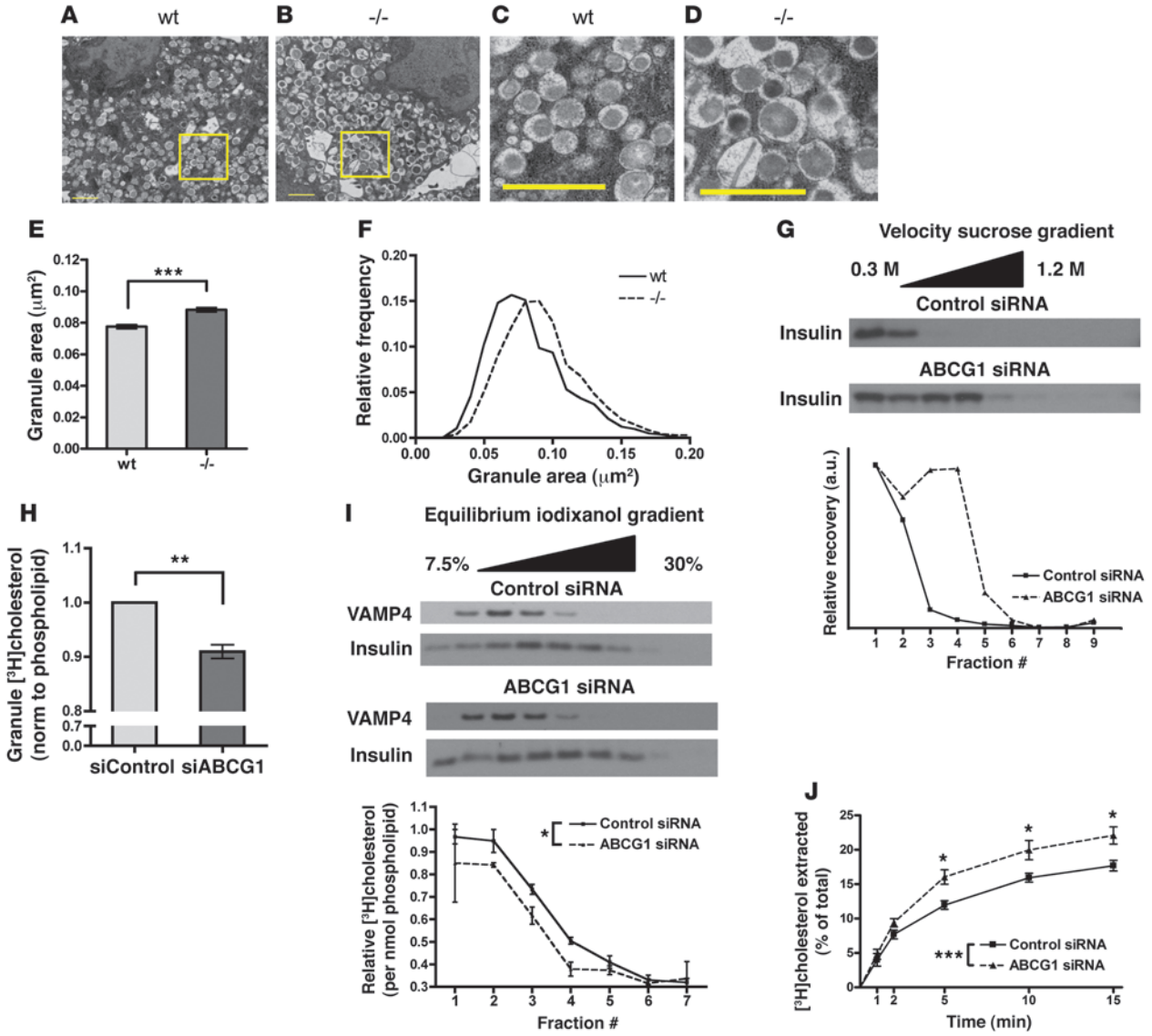

Figure 5

ABCG1 regulates secretory compartment cholesterol content. (**A**–**D**) WT and *Abcg1*$^{-/-}$ islets were isolated, and transmission electron microscopy was performed to analyze granule morphology. Scale bars: 1 μm. Panels **C** and **D** are enlarged from the highlighted areas in **A** and **B**. (**E** and **F**) Quantification of membrane-bound granule areas. (**E**) Mean granule area ± 95% CI. (**F**) Relative frequency distribution of granule areas (*n* granules: WT = 1945, –/– = 1654; *n* images: WT = 7, –/– = 6). (**G**) MIN6 cells were treated with control or ABCG1 siRNA. 60 hours following knockdown, cells were homogenized, and the postnuclear supernatant was subjected to velocity gradient centrifugation. (**H** and **I**) Measurements of granule cholesterol. MIN6 cells were treated with control or ABCG1 siRNA, then incubated with [³H]cholesterol overnight to label the granule population. Following incubation, granule fractions were isolated and subfractionated on continuous density gradients. Subfractions were assayed for [³H]cholesterol and phospholipid. (**H**) Total cholesterol content of the granule fraction; 4 independent experiments. (**I**) Western blotting for the immature granule marker VAMP4 and insulin in the subfractions. The plot below represents the [³H]cholesterol relative to phospholipid across the gradients; 2 independent experiments. (**J**) Assessment of relative plasma membrane cholesterol. MIN6 cells were treated with control or ABCG1 siRNA and labeled overnight with [³H]cholesterol. Cells were then cooled to 10°C to prevent membrane recycling, and surface accessible cholesterol was extracted with methyl-β-cyclodextrin. Extraction rate was monitored over 15 minutes and normalized to total cellular [³H]cholesterol (*n* = 8; 2 independent experiments). Data are presented as mean ± SEM. **P* < 0.05; ***P* < 0.01; ****P* < 0.001.

ditions, ABCG1 does not detectably regulate total β cell cholesterol content and that alterations in whole-cell cholesterol content do not mediate impairment of insulin secretion in ABCG1 deficiency.

ABCG1 mainly localizes to the regulated secretory pathway. In an effort to identify the site of secretory impairment in ABCG1 deficiency, we investigated the subcellular localization of ABCG1 in pancreatic β cells. Recent studies in other cell types have suggested that ABCG1 may be mostly concentrated intracellularly (13, 14). Because deficiency of ABCG1 did not impair cellular cholesterol efflux (Figure 3), we hypothesized that β cell ABCG1 might also be primarily intracellular. The distribution of endogenous ABCG1 was assessed using multiple approaches including

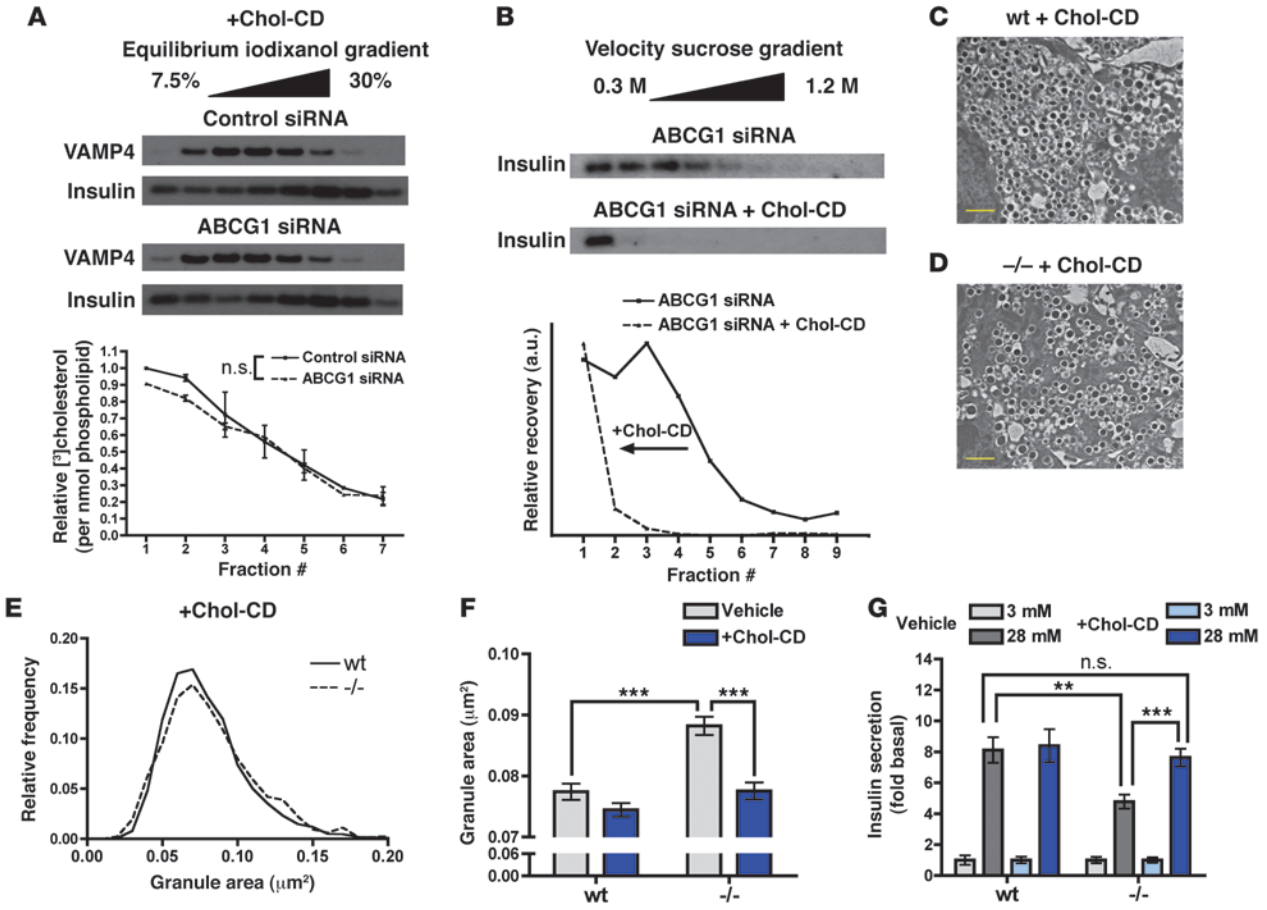

Figure 6

Exogenous cholesterol restores granule morphology and rescues insulin secretion in ABCG1 deficiency. (**A** and **B**) MIN6 cells were treated with control or ABCG1 siRNA and 36 hours after treatment were incubated overnight with 20 μg/ml soluble cholesterol (+Chol-CD). (**A**) [^{3}H]Cholesterol was included in the media and chol-CD, and granule [^{3}H]cholesterol content relative to phospholipid was assayed as in Figure 5I. (**B**) Velocity gradient centrifugation of MIN6 cells with knockdown of ABCG1, treated overnight with chol-CD. (**C**–**F**) WT (**C**) and *Abcg1*$^{-/-}$ islets (**D**) were treated overnight with chol-CD, and then transmission electron microscopy was performed to assess granule morphology. Scale bars: 1 μm. (**E**) Frequency distribution of granule areas from chol-CD–treated islets shown in **C** and **D** (*n* granules: WT = 2345, –/– = 2126; *n* images: WT = 6, –/– = 5). (**F**) Mean granule areas (± 95% CI) from vehicle (as shown in Figure 5) and chol-CD–treated WT and *Abcg1*$^{-/-}$ islets. (**G**) Glucose-stimulated insulin secretion in WT and *Abcg1*$^{-/-}$ islets treated with vehicle or chol-CD (*n* = 11–14, groups of 50 islets; 3 independent experiments). All fractionation studies are representative of 2–3 independent experiments. Data are presented as mean ± SEM. $^{**}P < 0.01$; $^{***}P < 0.001$.

subcellular fractionation, surface biotinylation, and confocal immunofluorescence microscopy. To our surprise, differential centrifugation of MIN6 cells indicated that a significant proportion of ABCG1 was recovered in the granule-enriched fraction and that it cofractionated with the granule marker secretogranin (SG) and not the plasma membrane marker Na/K-ATPase (Figure 4A). To distinguish whether ABCG1 was actually associated with granules and not with a variety of other organelles that are potential contaminants, we subfractionated the enriched granule fraction on 2 separate density gradients and compared the distribution of ABCG1 to a variety of organelle markers. Western blotting of fractions from both density gradients indicated that ABCG1 comigrated quite closely with the mature granule markers secretogranin and insulin. In contrast, syntaxin 6 (25) and vesicle-associated membrane protein 4 (VAMP4) (markers of the immature granules and trans-Golgi network [TGN]; refs. 25, 26), secretory carrier membrane protein SCAMP3 (a TGN and endosomal marker; refs. 27, 28), and lysosomal-associated membrane protein 1 (LAMP1, a late endosomal/lysosomal marker) were all restricted to lower densities (Figure 4, B–C, including densitometry profiles). These results suggest that ABCG1 resides to a substantial extent in the regulated secretory pathway as a membrane protein. Similar results were obtained upon fractionation of the rat adrenal chromaffin-derived PC12 cell line (Supplemental Figure 4), suggesting that ABCG1 may mark the regulated secretory pathway in multiple neuroendocrine cell types.

We also fractionated isolated C57BL/6 mouse islets. Results showed similar corecovery of ABCG1 and insulin in the granule-enriched fraction (Figure 4D). Subsequent centrifugation of this fraction over 1.5 M sucrose (29) revealed partial resolution of ABCG1 and insulin in that ABCG1 distributed 75%/25% between the interface (<1.5 M) and pellet (>1.5 M), whereas insulin distributed 50%/50% (Figure 4D).

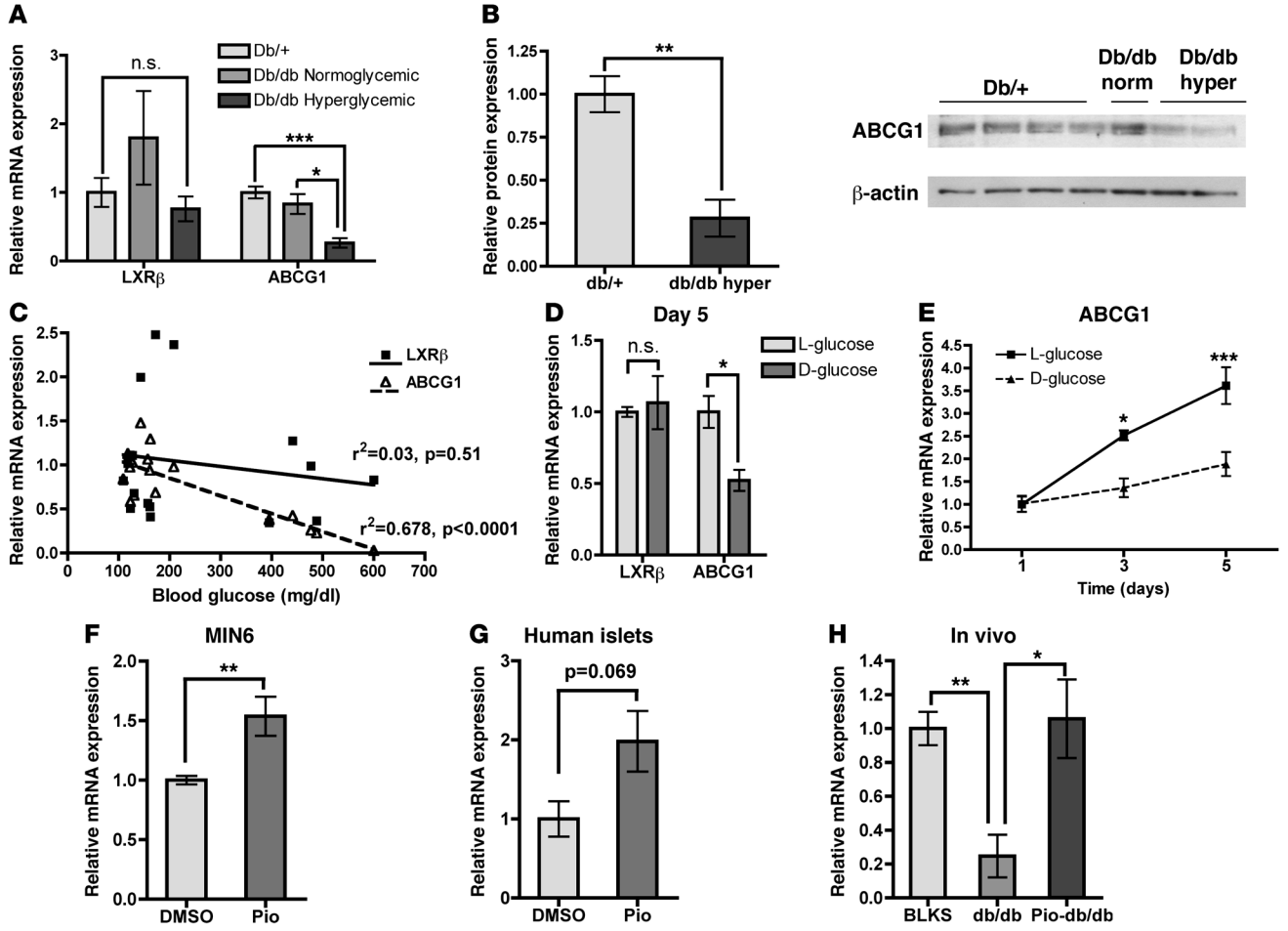

Figure 7

Islet ABCG1 expression is decreased in hyperglycemia and rescued by pioglitazone in vitro and in vivo. (**A**–**C**) Islets were isolated from hyperglycemic db/db, normoglycemic db/db, and db/+ control littermates, and mRNA (**A**, **C**) and protein (**B**) were harvested (n = 10 [db/+]; 2 [db/db normoglycemic]; 5 [db/db hyperglycemic]). (**A**) qRT-PCR for ABCG1 and LXRβ, the main transcriptional regulator of ABCG1 in islets. (**B**) Western blot for ABCG1. db/db norm, normoglycemic; db/db hyper, hyperglycemic. (**C**) Linear regression analysis of the correlations between islet mRNA levels of ABCG1 and LXRβ, and random blood glucose. (**D** and **E**) Isolated mouse islets were cultured for 1, 3, or 5 days in either 25 mM D-glucose or the nonmetabolizable L-glucose control (5.5 mM D-glucose + 19.5 mM L-glucose), mRNA was isolated, and qRT-PCR was performed (n = 3, representative of 3 independent experiments). (**D**) Relative expression of LXRβ and ABCG1 after 5 days in culture. (**E**) Time course of ABCG1 expression in response to glucose in culture. (**F**) MIN6 cells were treated for 24 hours with 10 μM pioglitazone, and *ABCG1* mRNA levels were measured (n = 6, from 2 independent experiments). (**G**) Isolated human islets from a cadaveric nondiabetic donor were treated for 24 hours with 5 μM pioglitazone, and *ABCG1* mRNA levels were measured (n = 4). (**H**) Db/db mice were treated with either vehicle or pioglitazone (Pio-db/db, 20 mg/kg body weight) for 6 weeks, islets were isolated, and *ABCG1* mRNA was measured. BLKS is the control background strain (n = 5, BLKS control; 3, db/db; 7, Pio-db/db). Data are presented as mean ± SEM. *P < 0.05; **P < 0.01; ***P < 0.001.

As a second methodology, and to directly address any potential localization of ABCG1 to the plasma membrane, we performed surface biotinylation experiments in MIN6 cells. As positive and negative controls, we compared biotinylation of the plasma membrane marker Na/K-ATPase and the cytoplasmic protein γ-adaptin. Results from these studies showed that only approximately 10%–12% of ABCG1 was surface labeled, whereas essentially all of Na/K-ATPase and none of γ-adaptin were detected (Figure 4E). These studies support the results from the cell fractionation experiments and demonstrate that the bulk of ABCG1 in β cells is intracellular.

Finally, we directly addressed the colocalization of ABCG1 with insulin in MIN6 cells using dual immunofluorescence staining (Figure 4, F–K). As detection of endogenous ABCG1 protein by this method has proved difficult in other cell types, we used confocal microscopy to allow better spatial resolution and minimize background, and we validated the specificity of staining by modulating ABCG1 levels using siRNA and LXR agonism. Staining of control-, ABCG1 siRNA–, and LXR agonist–treated samples showed that ABCG1 immunofluorescence was reduced by ABCG1 siRNA and induced by LXR agonism in parallel with ABCG1 protein levels as assessed by Western blot in identically treated samples (Supplemental Figure 5A), demonstrating specificity of staining for ABCG1. Examination of dual stained cells at high resolution revealed significant colocalization of ABCG1 and insulin in cytoplasmic puncta (Figure 4, F–K). Importantly, confocal z-stack series imaging showed that the colocalization extended through-

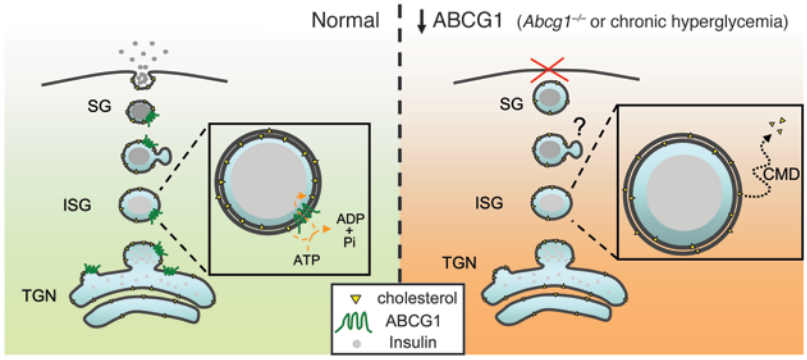

Figure 8

Proposed model of ABCG1 localization and action in the regulation of granule cholesterol content and insulin secretion. ABCG1 localizes to the regulated secretory pathway and acts to maintain secretory granule cholesterol, perhaps by redistributing granule membrane cholesterol to the inner leaflet, thereby regulating membrane curvature and restricting cholesterol exit via carrier-mediated diffusion to other cellular sites. This activity is analogous to that of other intracellular ABC transporters, which move their respective substrates into the lumen of the organelles in which they reside. In ABCG1 deficiency, cholesterol redistributes out of the granules; the granules are subsequently enlarged, and their release is impaired. SG, secretory granule; ISG, immature secretory granule, TGN, trans-Golgi network; CMD, carrier-mediated diffusion.

out the depth of the sample, demonstrating that these are localized to the same (not adjacent but overlapping) structures (Supplemental Figure 5C). Additionally, costaining for the ER chaperone BiP and ABCG1 showed no colocalization (Supplemental Figure 5B), further demonstrating the specific intracellular colocalization of ABCG1 with insulin. In aggregate, localization data gathered from multiple methodologies demonstrates consistently that the bulk of ABCG1 protein localizes to insulin granules.

Loss of ABCG1 leads to enlarged insulin granules with decreased cholesterol content. In light of the realization that ABCG1 largely resides in the regulated secretory pathway, we sought insight into its function in this compartment. Using transmission electron microscopy (TEM) on WT and *Abcg1*$^{-/-}$ islets, we noticed an apparent increase in size of β cell granules where the characteristic insulin crystal cores were surrounded by enlarged electron-lucent haloes (Figure 5, A–D). Measurements made on images documented this as a significant increase in mean granule membrane delimited cross-sectional area (Figure 5E) and as a rightward shift when plotted as a frequency distribution (Figure 5F). TEM analysis of adrenal chromaffin cells from *Abcg1*$^{-/-}$ mice showed a similar shift in size distribution as compared with WT (Supplemental Figure 6), further supporting a general role for ABCG1 in multiple neuroendocrine cell types.

To complement these observations in a separate cell system, we used siRNA-mediated knockdown of ABCG1 in MIN6 cells and subjected cell homogenates to velocity sucrose gradient ultracentrifugation. Western blotting of fractions for insulin revealed greater migration into the gradient of granules from the ABCG1-deficient cells than from control cells, indicative of increased granule size (Figure 5G, including densitometry).

Interestingly, the TGN and secretory granule membranes are known to have a relatively high cholesterol content (30, 31), which has been shown to be important for secretory granule function. Some granule proteins associate with cholesterol-rich sites of budding in the TGN (31, 32), and cholesterol ultimately is required for membrane fusion during exocytosis (33). Furthermore, in mouse models of Smith-Lemli-Opitz syndrome (SLOS) and lathosterolosis, in which cholesterol biosynthesis is impaired, secretory granule morphology is remarkably similar to what we have observed in ABCG1 deficiency (34). Since ABCG1 activity is thought to alter membrane cholesterol distribution, we hypothesized that it may regulate granule cholesterol content. To assess this possibility, we performed siRNA knockdown of ABCG1 in MIN6 cells, labeled them with [^{3}H]cholesterol overnight, isolated the granule-enriched fractions, subfractionated these on continuous density gradients, and assayed the recovery of [^{3}H]cholesterol. We normalized these results to phospholipid as a measure of total membrane. The cholesterol content of the granule fraction from ABCG1-deficient cells was significantly reduced by an average of approximately 10% (Figure 5H). This outcome was consistent across 4 independent experiments. Importantly, whole-cell [^{3}H]cholesterol labeling was equivalent between control and ABCG1 knockdown cells (Supplemental Figure 7A), so these differences were not due merely to changes in [^{3}H]cholesterol uptake.

Notably, profiles of cholesterol recovery across granule density gradients indicate that this reduction in granule cholesterol in ABCG1 deficiency may be restricted to lower density granules and that cholesterol progressively declined at higher densities in both groups (Figure 5I). Incubation with [^{3}H]cholesterol for an extended 48-hour period produced essentially identical results, indicating that the decline at higher densities is unlikely to reflect inaccessibility of these more dense granules to radiolabel. Furthermore, though there may be some contamination by other organelles, the recoveries of insulin and phospholipid mirror one another across the gradients, suggesting that insulin granules are the major source of membrane lipid across the gradients (Supplemental Figure 7B). The underlying basis for the variations in cholesterol content at different densities remains the subject of ongoing investigation.

One important consideration is that if granule cholesterol is reduced but total cellular cholesterol remains unchanged (Figure 3F), then the lost granule cholesterol must redistribute to another organelle. Therefore, in order to corroborate our findings and further evaluate the role of ABCG1 in β cell subcellular cholesterol distribution, we considered the cholesterol content of 2 main candidate organelles: the ER and the plasma membrane. Transcriptional profiling of cholesterol-regulated genes (Figure 3G), an exquisitely sensitive measure of ER cholesterol content, showed no difference between genotypes, so it does not appear that granule cholesterol redistributes to the ER pool. To assess relative plasma membrane cholesterol, we treated MIN6 cells with control or ABCG1 siRNA, labeled them overnight with [^{3}H]cholesterol, then chilled the cells to 10°C to inhibit membrane recycling, and measured the rate of plasma membrane cholesterol extraction by methyl-β-cyclodextrin (MβCD), similar to previous protocols with minor modifications (35–37). Results from these studies showed a significant increase in the rate of plasma membrane cholesterol extraction by MβCD from ABCG1-deficient cells (Figure 5J), indicative of an increase in accessible cholesterol relative to control. Importantly, this increase cannot be due to impaired removal of plasma membrane cholesterol

because efflux to physiological acceptors was not impaired (Figure 3, C–E). Together, these data confirm the findings from measures of granule cholesterol, and they suggest that the plasma membrane is at least one site of granule cholesterol redistribution.

Exogenous cholesterol restores insulin granule cholesterol content and morphology and rescues insulin secretion in ABCG1 deficiency. To further interrogate the link between reduced granule cholesterol, altered granule morphology, and impaired insulin secretion in ABCG1 deficiency, we undertook a series of experiments utilizing addition of exogenous cholesterol with cholesterol-loaded methyl-β-cyclodextrin (chol-CD). Treatment of ABCG1-deficient MIN6 cells with chol-CD overnight restored granule cholesterol content to the level observed in control cells (Figure 6A). Strikingly, exogenous cholesterol also restored insulin granule size, as indicated by the leftward shift of insulin recovered in velocity gradient fractions (Figure 6B; compare with Figure 5G). Similarly, cholesterol addition to isolated *Abcg1*$^{-/-}$ islets restored a near-normal granule size distribution as measured from TEM images (Figure 6, C–E; mean granule areas from untreated and chol-CD–treated islets from both genotypes are shown together in Figure 6F). Finally, addition of exogenous cholesterol also markedly improved insulin secretion in *Abcg1*$^{-/-}$ islets (Figure 6G), and paralleled the changes in granule area (Figure 6F). Together, these results indicate that ABCG1 is a novel regulator of cholesterol content within the regulated secretory pathway and that reduced granule cholesterol is one underlying cause of impaired insulin secretion in ABCG1 deficiency.

Islet ABCG1 expression is reduced in a mouse model of diabetes and increased by pioglitazone in vitro and in vivo. Prior studies from our group have shown that ABCG1 expression is reduced in macrophages isolated from diabetic mice (15) and humans (16) and that this reduction could be recapitulated with chronic high glucose in vitro (15). To determine whether this phenomenon occurs similarly in β cells, we isolated islets from diabetic db/db mice and control db/+ mice and measured ABCG1 levels. Hyperglycemic db/db mice showed a marked reduction in *ABCG1* mRNA (Figure 7A) and protein (Figure 7B), while normoglycemic db/db mice did not differ from db/+ controls. Plotting islet *ABCG1* mRNA as a function of blood glucose revealed a significant negative correlation as assessed by linear regression analysis (Figure 7C). Additionally, chronic culture of WT islets in high D-glucose in vitro led to significant reductions in *ABCG1* mRNA at 3 and 5 days of treatment, as compared with the nonmetabolizable L-glucose control (Figure 7, D and E). Together, these results demonstrate that islet ABCG1 expression is reduced in a murine model of diabetes, and they suggest that this downregulation may be mediated by chronic high glucose. Furthermore, these data suggest that reduced ABCG1 expression may be one mechanism contributing to progressive β cell dysfunction in chronic hyperglycemia.

TZDs such as rosiglitazone and pioglitazone are commonly used drugs for the clinical treatment of diabetes and have numerous beneficial effects on β cell function (21, 38), including significantly elevated cellular granule content (39). A recent elegant study by Brunham et al. showed that ABCA1 in β cells was required for the whole-animal metabolic response to rosiglitazone (6), which suggests that β cell cholesterol homeostasis may be a critical factor in this process. Importantly, ABCG1 is a known transcriptional target of PPARγ agonism in other tissues (17, 18). To determine whether PPARγ could upregulate ABCG1 expression in β cells, we treated MIN6 cells for 24 hours with pioglitazone and measured *ABCG1* mRNA. This treatment significantly upregulated ABCG1 expression (Figure 7F), indicating that pioglitazone can activate β cell ABCG1 expression in a cell-autonomous manner. We observed a similar increase in human islets treated with pioglitazone in vitro (Figure 7G), indicating that this effect extends to primary human cells. We then asked whether β cell ABCG1 could be regulated by PPARγ agonism in the context of β cell dysfunction. We measured ABCG1 expression in islets from db/db mice treated for 6 weeks with pioglitazone (Pio-db/db). Pio-db/db mice had significantly reduced random blood glucose, improved glucose tolerance, and increased serum insulin levels as compared with untreated db/db mice, indicative of markedly improved β cell function (21). Interestingly, islet ABCG1 expression in Pio-db/db mice was increased 4-fold over untreated db/db mice and was indistinguishable from nondiabetic control levels (Figure 7H). This demonstrates that the transcriptional machinery required to upregulate ABCG1 expression is intact in the failing β cell, and it suggests that increased β cell ABCG1 may contribute to improved β cell function in response to TZDs.

Discussion

Cellular cholesterol homeostasis has emerged as an important modulator of insulin secretion, and altered β cell cholesterol homeostasis has been implicated in islet dysfunction in disease and the response to pharmacologic therapy. ABCG1 has been shown to regulate cholesterol content in other cell types, but its role in β cell function has not been explored. The studies reported here extend the role of ABCG1 in cellular cholesterol homeostasis to β cells and link this to modulation of insulin secretion. More importantly, they demonstrate the primary localization of ABCG1 to an intracellular compartment and subsequently uncover a role for ABCG1-mediated cholesterol transport in the function of that compartment, the regulated secretory pathway. These findings have important implications, not only for how we understand β cell function and regulated secretion, but also for how we assess the general role of ABCG1 in cellular cholesterol homeostasis.

The first data implicating ABCG1 in β cell function came from our studies of glucose metabolism in WT and *Abcg1*$^{-/-}$ mice, wherein *Abcg1*$^{-/-}$ mice had impaired glucose tolerance and insulin secretion, consistent with a primary β cell defect (Figure 1). In parallel with these in vivo observations, *Abcg1*$^{-/-}$ islets had decreased insulin secretion in vitro. This defect appeared to be distal to glucose sensing and to extend to both first- and second-phase insulin secretion (Figure 2), suggesting that loss of ABCG1 leads to impairment of later steps in insulin granule release, perhaps at the level of granule priming or membrane fusion.

These secretory defects are similar to those shown in LXRβ-deficient islets (40), which have an 80% reduction in islet *ABCG1* mRNA, and in ABCA1-deficient islets (6). However, both LXRβ- and ABCA1-deficient islets had some measure of either cholesterol or neutral lipid accumulation. Surprisingly, we found no change in β cell cholesterol efflux or content in ABCG1 deficiency (Figure 3). In order to better understand how loss of ABCG1 could impair insulin secretion without an increase in cellular sterol content, we utilized multiple methodologies to assess the subcellular localization of endogenous ABCG1 protein in both MIN6 and primary mouse β cells (Figure 4). Surprisingly, only about 10% of ABCG1 was present on the cell surface, whereas most of the remaining 90% localized to insulin granules. This localization may be limited to a subset of insulin granules, as both immunofluorescence and density gradient fractionation of MIN6 cells and islets showed a proportion of insulin staining without significant ABCG1. To

the extent that increased granule density correlates with increased granule maturity (41), these ABCG1-deficient granules may be older or more mature. This raises the interesting possibility that ABCG1 may not be retained throughout the granule lifetime, though its retention substantially exceeds that of VAMP4 and syntaxin 6 — membrane components that are restricted to immature granules (25, 26). In any event, ABCG1 is a long-term resident of the regulated secretory pathway; how it enters and possibly exits the pathway remain subjects for further investigation.

In light of this subcellular localization of ABCG1, we assessed granule morphology and cholesterol content in ABCG1 deficiency. Interestingly, the granule morphology in *Abcg1*$^{-/-}$ islets resembled that seen in mice with impairments in cholesterol biogenesis (34), and measurements of granule lipid content showed decreased granule cholesterol in ABCG1-deficient cells (Figure 5). Profiling of granule cholesterol content across density gradients suggested that this decrease may be limited to less dense granules, as the difference in granule cholesterol between control and ABCG1 siRNA was blunted at higher densities. This is consistent with a possible restriction of ABCG1 to this lower density granule subset. Importantly, addition of exogenous cholesterol restored secretory compartment cholesterol and granule size and rescued insulin secretion in *Abcg1*$^{-/-}$ islets (Figure 6), indicating that this reduced granule cholesterol is at least one mechanism of impaired insulin secretion in ABCG1 deficiency. Granule cholesterol deficiency could negatively impact the regulated secretory pathway at various levels. Interestingly, cholesterol itself supports lipid bilayer rearrangement during membrane fusion, and studies in a cell-free system showed that a reduction of granule membrane cholesterol by only 10% reduced exocytotic events to 60%–70% of control (33): both similar values to what we observe in ABCG1 deficiency. Cholesterol-enriched membranes also support SNARE-mediated exocytosis (42), and reduced granule cholesterol content could alter the assembly or function of SNARE complexes. Alternatively, the impaired insulin secretion could reflect retention of a negative regulator of exocytosis during granule maturation (26), particularly since cholesterol contributes to assembly of membrane microdomains during vesicle budding and the granule morphology we observe is similar to that observed in other examples of impaired membrane sorting (43).

The precise cellular mechanisms for ABCG1 action in cholesterol homeostasis are unknown. The best evidence on ABCG1-mediated cholesterol efflux underscores 2 points: first, ABCG1 probably has to be at the plasma membrane to promote cholesterol efflux (14, 44); and second, ABCG1 redistributes membrane cholesterol to efflux accessible pools (44). Most of the plasma membrane cholesterol resides in the cytoplasmic leaflet (45), and one mechanism whereby ABCG1 could promote cholesterol efflux would be to facilitate its redistribution to the outer leaflet. In the secretory granule, this would correspond topologically to the inner (lumenal) leaflet. Interestingly, other intracellular ABC transporters act to drive their substrates into their respective intracellular compartments in a similar manner (46, 47), and in fact the *Drosophila* homolog of ABCG1, *white*, localizes to pigment granule membranes in the fly eye, where it facilitates uptake of pigment precursors into the granule (48). Thus, we propose that ABCG1 maintains secretory granule cholesterol by facilitating its concentration in the granule membrane inner leaflet, thereby limiting cholesterol dispersion to other cellular sites (Figure 8). This concept is particularly interesting in the β cell because of the relative proportion of cellular lipid that is partitioned to the granule membrane. Stereological analysis of islets showed that each β cell contains approximately 9,000 granules and that the total surface area of these granules amounts to 4.5 times that of the plasma membrane (49). Furthermore, the cholesterol content of granule membranes is similar to that in the plasma membrane (50), so though the plasma membrane may contain the bulk of cellular-free cholesterol in other cell types (51), in the β cell, the granule accounts for a substantial portion of the cholesterol pool. It is perhaps not quite as surprising then that a cholesterol transporter localizes to this compartment where it can play a pivotal role in cholesterol handling. This realization also has important implications for how we interpret measures of whole-cell cholesterol content in β cells and underscores the importance of assessing subcellular cholesterol distribution.

Given our data on the role of ABCG1 in insulin secretion, we sought to extend previous findings on the regulation of ABCG1 expression in other cell types to β cells (Figure 7). As in macrophages, ABCG1 expression was significantly reduced in islets isolated from hyperglycemic db/db mice, and chronic culture of isolated islets in high glucose produced a similar effect. These results suggest that islet ABCG1 expression is probably reduced later in disease when hyperglycemia has already ensued and that this effect might propagate metabolic dysfunction in a positive feedback cycle, reminiscent of β cell failure in advanced disease. The mechanism for downregulation of ABCG1 expression by high glucose is unclear. Importantly, mRNA levels of LXRβ, the primary regulator of ABCG1 expression in islets, were unchanged, whereas mRNAs of other transcriptional targets of LXR (ABCA1 and SREBP-1c) were downregulated (Supplemental Figure 8), consistent with altered LXR activity. This effect could be mediated by posttranscriptional or posttranslational modifications of LXR (52, 53); similar mechanisms have been shown in islets for the transcription factors Pdx1 and MafA (54, 55). Alternatively, reduced LXR activity may reflect reduced ligand availability, as shown during T lymphocyte expansion (56). Interestingly, pioglitazone increased islet ABCG1 expression in vitro and restored islet ABCG1 expression to normal levels in diabetic animals. Though TZDs are widely used to treat metabolic dysfunction in diabetes, clinical data have generated controversy as to the efficacy of TZDs in prevention of cardiovascular disease and mortality (57). Based on our data, at least at the level of the β cell, specific targeting of ABCG1 expression may be a viable alternative approach. Future studies aimed at testing this hypothesis will require β cell–specific deletion or overexpression of ABCG1 in vivo in models of diabetes.

In summary, we have shown here that ABCG1 has a critical intracellular role in pancreatic β cell function. Our paradigm indicates that ABCG1 does not modulate insulin secretion through regulation of total cellular cholesterol content, but instead through regulation of subcellular cholesterol distribution and maintenance of membrane cholesterol content in a cholesterol-rich organelle, the secretory granule. Furthermore, we have shown that modulation of islet ABCG1 expression may play an important role in diabetes pathogenesis and treatment. Many studies of ABCG1 in a variety of other cell types and biological processes, such as atherosclerosis, have produced unexpected and discrepant results that may not be explained simply by total cellular cholesterol accumulation (58, 59). Future studies addressing the subcellular localization and trafficking of ABCG1 in these other cell types will likely shed light on the mechanisms of ABCG1 action in diverse cellular processes and may thereby elucidate the roles of ABCG1 in human disease.

Methods

Mice. C57BL/6 mice and db/db C57BLKS mice were purchased from Jackson Laboratory. *Abcg1*$^{-/-}$ mice (19) were purchased originally from Deltagen. All mice were fed standard rodent chow, housed in microisolator cages in a pathogen-free facility, and maintained under a 14-hour light/10-hour dark cycle, with lights on at 6:30 am, lights off at 8:30 pm. For pioglitazone studies, pioglitazone was initially dissolved in ethanol at a mixture of 10% w/v, then diluted with PBS to a final ethanol concentration of 1.8%. Mice were given 20 mg/kg body weight pioglitazone in 400 μl ethanol/PBS (or ethanol/PBS vehicle alone) daily by oral gavage as described (21). All procedures were reviewed and approved by University of Virginia and Indiana University Laboratory Animal Care and Use Committee review boards.

In vivo metabolic testing. For glucose tolerance testing, mice were fasted overnight and challenged with D-glucose (1–3 g/kg body weight) via i.p. injection. For insulin tolerance testing, mice were fasted 4 hours and, between the hours of 2:00 and 3:00 pm, challenged with recombinant human insulin (0.75 U/kg body weight; Novolin R, Novo Nordisk). Blood glucose levels were measured via tail clip with a OneTouch Ultrasmart glucometer. Plasma insulin was measured using Ultrasensitive Mouse Insulin ELISA (ALPCO).

Islet isolation and cell culture. Primary mouse islets were isolated via intraductal collagenase (Roche) digestion and density centrifugation essentially as described previously (60). Following isolation, islets were hand picked and maintain in DMEM without phenol red, 5.5 mM glucose plus 10% (v/v) FBS (Sigma-Aldrich), and penicillin and streptomycin. Human islets were obtained from Beta-Pro LLC and upon arrival were placed in DMEM without phenol red, 5.5 mM glucose plus 10% (v/v) fetal bovine serum, and penicillin and streptomycin, and allowed to recover overnight before initiation of experiments. MIN6 cells were a gift of Chien Li (University of Virginia) and were maintained in DMEM with 15% FBS and penicillin and streptomycin. PC12 cells were maintained at 10% CO_2 in DMEM with 10% horse serum and 5% FBS (61). For in vitro studies with pioglitazone, cells were cultured in DMEM, 5.5 mM glucose plus 1% (v/v) lipoprotein-deficient fetal bovine serum (Biomedical Technologies) with either vehicle (DMSO) or 5–10 μM pioglitazone for 24 hours. For treatment with soluble cholesterol, cells were incubated overnight with 20 μg/ml cholesterol-loaded methyl-β-cyclodextrin (Chol-CD) (Sigma-Aldrich) in the presence of 10% (islets) or 15% (MIN6) FBS. Chol-CD was not included in the medium during GSIS in order to prevent acute cholesterol loading of the plasma membrane. Knockdown of ABCG1 in MIN6 cells was done with heteroduplex siRNA constructs (Dharmacon, L-040312) and using Lipofectamine RNAiMAX (Invitrogen) according to manufacturer instructions. 1.2×10^6 MIN6 cells were plated with 25–50 pmol of siRNA/well of a 6-well dish for protein harvest or fractionation, or 3×10^5 cells with 6.25–12.5 pmol siRNA/well of a 24-well dish for efflux assays. Experiments were performed 60 hours following initiation of siRNA unless otherwise described. For LXR agonism, T0901317 was from Caymen, and GW3965 was from Sigma-Aldrich.

Immunohistochemistry. Measurements of β cell mass were performed as described (62). Mice were euthanized and perfused through the heart with PBS and 4% paraformaldehyde. Fixed pancreata were embedded in paraffin, and 5 μM sections were stained with rabbit polyclonal anti-insulin antibody (1:500; Santa Cruz Biotechnology Inc.) and secondary antibody peroxidase conjugate to enable quantification of positive-stained areas. Digital images of each section at ×10 magnification were acquired on an Axio-Observer Z1 microscope (Zeiss) fitted with an AxioCam high resolution color camera. Relative β cell area was calculated using Axio-Vision Software.

In vitro insulin secretion and calcium measurements. Glucose- and potassium-induced insulin secretion were measured as described (23, 62). Islets (50 per sample) were treated according to specified experimental conditions, preincubated in 0 mM glucose HEPES-buffered Krebs-Ringer solution (KRB) for 1 hour, then incubated for 1 hour in 3 mM glucose KRB, followed by 1 hour in KRB containing either 30 mM KCl or 28 mM glucose. Following incubations, total islet insulin was extracted with acid ethanol. Insulin concentration in the media and extracts was measured using the Ultrasensitive Mouse Insulin ELISA from ALPCO. Insulin secretion was normalized to total insulin content. For measurements of first- and second-phase insulin secretion, islets were incubated in 3 mM glucose KRB plus 30 mM KCl for 5 minutes, followed by incubation in 28 mM glucose KRB for an additional 10 minutes. Intracellular calcium measurements were made using the ratiometric calcium dye fura-2 (63). Islets were loaded with 3 μM fura-2-acetoxymethylester (fura-2 AM) for 30 minutes, transferred to a low-volume chamber (Warner Instruments), mounted on the stage of an Olympus BX51WI fluorescence microscope, and subsequently perifused with 3 mM followed by 28 mM glucose KRB delivered by a peristaltic pump (Gilson) maintained at 37°C with an in-line heater (Warner Instruments). During perifusion, fura-2 AM was excited by xenon bulb light source, with sequential excitation at 340 and 380 nm and emission recorded at 510 nm. Relative Ca^{2+} concentration was determined by the ratio of emission from the 2 excitation wavelengths.

Cholesterol efflux and lipid analyses. Cholesterol efflux assays were performed as described with minor modifications (15). MIN6 cells were plated in 24-well culture dishes and treated according to experimental conditions. On the day of the experiment, cells were washed 3 times with DMEM, preincubated in DMEM plus 0.02% fatty acid–free bovine serum albumin (FAFBSA) for 2 hours, followed by incubation with media containing either FAFBSA alone or FAFBSA plus the lipoprotein acceptor, which, depending upon the experiment, was either 50 μg/ml HDL (Intracel) for 30 minutes to 8 hours, 5–100 μg/ml HDL for 4 hours, or 15 μg/ml human ApoAI (isolated as previously described in ref. 64) for 4 hours. Following incubation in acceptor media, the media were removed, cells were dried, and lipid was extracted overnight in isopropanol. [^{3}H]cholesterol in media and extract was quantified by liquid scintillation counting. HDL- or ApoAI-mediated cholesterol efflux was calculated by subtracting efflux to FAFBSA containing media from efflux to media with FAFBSA plus acceptor, and was normalized to cellular [^{3}H]cholesterol content. For plasma membrane cholesterol extraction assays, cells were treated as described above, but following the 2-hour preincubation period, cells were chilled to 10°C, extraction media containing 0.2% FAFBSA plus 10 mM methyl-β-cyclodextrin was added, and aliquots were taken and replaced with fresh media at 1, 2, 5, 10, and 15 minutes. Cells and samples were then processed as described above. For assessment of subcellular [^{3}H]cholesterol distribution, cells were labeled with 2 μCi/ml [^{3}H]cholesterol overnight, subjected to fractionation as described, and radioactivity was measured via scintillation counting. In experiments in which cells were treated with cholesterol-loaded methyl-β-cyclodextrin, both FBS and chol-CD were prelabeled for 1 hour at room temperature with equivalent amounts of [^{3}H]cholesterol to yield a final concentration of 2 μCi/ml [^{3}H]cholesterol. Cholesterol content was normalized to phospholipid content following extraction (65) and assay of lipid-derived inorganic phosphate (66). Total islet cellular cholesterol content was quantified by gas-liquid chromatography (67). MIN6 total cholesterol content was determined by enzymatic assay (WAKO). Triglyceride content was quantified using the Infinity Triglycerides Reagent enzymatic assay (Thermo Scientific).

Subcellular fractionation. MIN6 (29, 68) and PC12 (69) cells were fractionated using previously described procedures with minor modifi-

cations. Briefly, MIN6 cells were grown to 70%–80% confluence and homogenized by 10–12 passes through a 27-gauge needle in homogenization buffer (20 mM Tris-HCl, pH 7.4, 0.5 mM EDTA, 0.5 mM EGTA, 250 mM sucrose, 1 mM DTT, and 1:100 Sigma-Aldrich protease inhibitor cocktail). Homogenization efficiency was monitored by phase-contrast microscopy. Whole-cell homogenate was centrifuged at 900 *g* for 10 minutes to pellet nuclei and plasma membrane (PM). The post-nuclear supernatant (PNS) was spun at 5,400 *g* for 15 minutes, and the post-mitochondrial supernatant (PMS) was subsequently spun at 25,000 *g* for 20 minutes to pellet the granule-enriched fraction. The remaining supernatant was then spun at 100,000 *g* for 1 hour to pellet microsomes from cytosol. For PM collection, the nuclear/PM pellet was resuspended in 1 ml 0.25 M sucrose plus 2 ml 2 M sucrose, overlaid with 0.25 M sucrose, and subsequently spun at 113,000 *g* for 1 hour. The interface was collected, diluted, and pelleted at 8,000 *g* to generate the PM fraction. In preparation for equilibrium density gradient centrifugation (to separate on the basis of organelle density), the PMS was adjusted to 10 mM EDTA, and the granule-enriched fraction was sedimented onto either a high-density sucrose or iodixanol (OptiPrep; Nyegard) cushion. The collected fraction was loaded on either a continuous sucrose (0.5–2.0 M) or iodixanol (7.5%–30%) gradient and spun at 150,000 g_{max} for 5 hours. For velocity sucrose gradient centrifugation (to separate on the basis of organelle size), the PNS was adjusted to 10 mM EDTA, loaded on a continuous sucrose gradient (0.3–1.2 M), and spun at 110,000 *g* for 1 hour. 1 ml fractions were collected, and the pellet (fraction 10), which included some whole cells and possibly organelle aggregates, was excluded from distribution analysis. Primary mouse islets were fractionated as previously described (29).

Immunofluorescence and surface biotinylation. Immunofluorescence staining and microscopy were performed as previously described (28). MIN6 cells were plated on tissue culture–treated glass chamber slides (Lab-Tek) and where applicable were treated with siRNA or T0901317 as described. Cells were fixed with 4% paraformaldehyde, quenched in PBS containing 50 mM glycine, and permeabilized in PBS plus 0.1% Triton X-100. Samples were blocked with 2% goat serum, labeled with primary antibodies to rabbit anti-ABCG1 (2–5 μg/ml), guinea pig anti-insulin (1:1500), and mouse anti-BiP (1:200), and subsequently labeled with Alexa Fluor–conjugated secondary antibodies (1:500; Alexa Fluor 488 for ABCG1, Alexa Fluor 647 for insulin and BiP). Images were acquired on a NikonC1 confocal microscope. Quantitative analysis of colocalization was done using the JACoP plug-in in ImageJ software (70).

Surface biotinylation of MIN6 cells was performed similarly to what was previously described (71). Cells were grown in 10 cm dishes, plated 3 days before the experiment, labeled on ice for 30 minutes with 1 mg/ml EZ-Link Sulfo-NHS-SS-Biotin (Thermo Scientific) in Ca^{2+}- and Mg^{2+}-containing PBS, pH 8; quenched with 1% BSA, and lysed and scraped in 0.1% NP-40 in PBS, 2 mM EDTA, 2.5 mM iodoacetamide, protease inhibitor cocktail (Roche), 1 ml per plate. A portion of the lysate was then removed, and biotinylated proteins were precipitated with Neutravidin beads for 2 hours at room temperature. Following binding, beads were washed and bound proteins were eluted with sample buffer plus DTT. SDS-PAGE and Western blotting were performed from gels loaded with 3 different volumes each of lysate and bead eluate to confirm proportionate antigen recovery, and blots were developed and quantified using a Fuji LAS-3000 imager and ImageQuant software.

Electron microscopy. Primary mouse islets were isolated, fixed in phosphate-buffered 4% PFA, 2.5% glutaraldehyde, post-fixed with 1% osmium tetroxide, dehydrated in acetone, and embedded in EPON. Ultrathin sections were stained with aqueous uranyl acetate and lead citrate. Dissected mouse adrenal glands were similarly processed except that initial fixation was in 0.1 M cacodylate-buffered 2% formaldehyde, 3% glutaraldehyde, and the osmium used for post-fixation contained 0.1% potassium ferrocyanide. Specimens were stained in-block with 0.5% uranyl acetate, pH 6, prior to dehydration and embedding. Digital images were acquired using a JEOL 1230 electron microscope in the University of Virginia Advanced Microscopy Facility and analyzed using Image-Pro software (Media Cybernetics Inc). For islet granule analysis, insulin granules were identified by the characteristic appearance of their zinc-insulin condensed core with surrounding halo. For chromaffin granule analysis, care was taken to focus on a single cell type in which granules had dense cores surrounded by membrane-limited haloes.

Western blot and qRT-PCR. Western blotting and quantitative RT-PCR (qRT-PCR) analysis were performed essentially as previously described (15, 72). For Western blotting, RIPA buffer (50 mM TrisHCl, pH 8.0, 150 mM NaCl, 1% Igepal, 10 mM NaF, 2 mM Na_3VO_4, and Sigma-Aldrich proteases inhibitor cocktail) was added to cells to generate whole-cell lysates. Total protein was quantified using a protein assay kit (Bio-Rad). Proteins were separated by SDS-PAGE and transferred to nitrocellulose (materials and buffers from Invitrogen); membranes were washed with Tris-buffered saline with 0.1% (v/v) Tween-20 (TBST) and blocked in TBST with 2.5% milk (w/v). Proteins were detected using specific primary antibody and horseradish peroxidase–conjugated secondary antibody, and visualized by chemiluminescence. Antibodies used were obtained as follows: ABCG1 (Novus), β-actin (Santa Cruz Biotechnology Inc.), BiP (Stressgen), insulin (rabbit, Santa Cruz Biotechnology Inc.; guinea pig, Linco), LAMP1 (Developmental Studies Hybridoma Bank, University of Iowa), Na/K-ATPase (Upstate), SCAMP3 (generated as described; ref. 73), secretogranin (isoform II; Biodesign), syntaxin 6 (Stressgen), and VAMP4 (Affinity Bioreagents). For qRT-PCR, RNA was isolated using the RNeasy Mini Kit (QIAGEN) as per manufacturer's instructions. RNA was quantified, and cDNA from equivalent starting material for each sample was synthesized using the iScript cDNA Synthesis Kit (Bio-Rad). Total cDNA was then diluted 1:10 in water, and a serial dilution standard and negative control (no reverse transcriptase) were used. A Bio-Rad MyIQ Single Color Real-Time PCR Detection System and the Bio-Rad iQ SYBR Green Supermix were used to run the reactions and quantify.

Statistics. Data were analyzed by ANOVA, 2-tailed Student's *t* tests, or linear regression, where appropriate, using GraphPad Prism4 statistical software. All results are presented as mean ± SEM unless otherwise specified.

Acknowledgments

The authors would like to acknowledge M.D. Skaflen and A.K. Gebre for their expert technical assistance, J.A. Redick and S. Guillot for their electron microscopy services, and C.S. Nunemaker for helpful discussion. J.M. Sturek was supported by an NIGMS-NHLBI predoctoral fellowship. This work was supported in part by grants from the NIH (P01 HL55798 and R01 HL085790 to C.C. Hedrick; R01 DK073380 to J.D. Castle; K08 DK 80225 to C. Evans-Molina; R01 HL094525 and P01 HL049373 to J.S. Parks; and R01 DK60581 to R.G. Mirmira) and an investigator-initiated grant from Takeda Pharmaceuticals to R.G. Mirmira.

Received for publication September 29, 2009, and accepted in revised form April 14, 2010.

Address correspondence to: Catherine Hedrick, La Jolla Institute for Allergy and Immunology, Division of Inflammation Biology, 9420 Athena Circle, La Jolla, California 92037, USA. Phone: 858.752.6604; Fax: 858.752.6985; E-mail: hedrick@liai.org.

1. Ikonen E. Cellular cholesterol trafficking and compartmentalization. *Nat Rev Mol Cell Biol*. 2008;9(2):125–138.
2. Perley MJ, Kipnis DM. Plasma insulin responses to oral and intravenous glucose: studies in normal and diabetic sujbjects. *J Clin Invest*. 1967;46(12):1954–1962.
3. Prentki M, Nolan CJ. Islet beta cell failure in type 2 diabetes. *J Clin Invest*. 2006;116(7):1802–1812.
4. Wilson PW, McGee DL, Kannel WB. Obesity, very low density lipoproteins, and glucose intolerance over fourteen years: The Framingham study. *Am J Epidemiol*. 1981;114(5):697–704.
5. Brunham LR, Kruit JK, Verchere CB, Hayden MR. Cholesterol in islet dysfunction and type 2 diabetes. *J Clin Invest*. 2008;118(2):403–408.
6. Brunham LR, et al. [beta]-cell ABCA1 influences insulin secretion, glucose homeostasis, and response to thiazolidinedione treatment. *Nat Med*. 2007;13(3):340–347.
7. Hao M, Head WS, Gunawardana SC, Hasty AH, Piston DW. Direct effect of cholesterol on insulin secretion: a novel mechanism for pancreatic {beta}-cell dysfunction. *Diabetes*. 2007;56(9):2328–2338.
8. Vikman J, Jimenez-Feltstrom J, Nyman P, Thelin J, Eliasson L. Insulin secretion is highly sensitive to desorption of plasma membrane cholesterol. *FASEB J*. 2009;23(1):58–67.
9. Xia F, et al. Inhibition of cholesterol biosynthesis impairs insulin secretion and voltage-gated calcium channel function in pancreatic beta-cells. *Endocrinology*. 2008;149(10):5136–5145.
10. Wang N, Lan D, Chen W, Matsuura F, Tall AR. ATP-binding cassette transporters G1 and G4 mediate cellular cholesterol efflux to high-density lipoproteins. *Proc Natl Acad Sci U S A*. 2004;101(26):9774–9779.
11. Vedhachalam C, Ghering AB, Davidson WS, Lund-Katz S, Rothblat GH, Phillips MC. ABCA1-induced cell surface binding sites for ApoA-I. *Arterioscler Thromb Vasc Biol*. 2007;27(7):1603–1609.
12. Vedhachalam C, et al. Mechanism of ATP-binding cassette transporter A1-mediated cellular lipid efflux to apolipoprotein A-I and formation of high density lipoprotein particles. *J Biol Chem*. 2007;282(34):25123–25130.
13. Tarr PT, Edwards PA. ABCG1 and ABCG4 are coexpressed in neurons and astrocytes of the CNS and regulate cholesterol homeostasis through SREBP-2. *J Lipid Res*. 2008;49(1):169–182.
14. Wang N, Ranalletta M, Matsuura F, Peng F, Tall AR. LXR-induced redistribution of ABCG1 to plasma membrane in macrophages enhances cholesterol mass efflux to HDL. *Arterioscler Thromb Vasc Biol*. 2006;26(6):1310–1316.
15. Mauldin JP, et al. Reduction in ABCG1 in Type 2 diabetic mice increases macrophage foam cell formation. *J Biol Chem*. 2006;281(30):21216–21224.
16. Mauldin JP, et al. Reduced expression of ATP-binding cassette transporter G1 increases cholesterol accumulation in macrophages of patients with type 2 diabetes mellitus. *Circulation*. 2008;117(21):2785–2792.
17. Akiyama TE, et al. Conditional disruption of the peroxisome proliferator-activated receptor {gamma} gene in mice results in lowered expression of ABCA1, ABCG1, and apoE in macrophages and reduced cholesterol efflux. *Mol Cell Biol*. 2002;22(8):2607–2619.
18. Li AC, et al. Differential inhibition of macrophage foam-cell formation and atherosclerosis in mice by PPARalpha, beta/delta, and gamma. *J Clin Invest*. 2004;114(11):1564–1576.
19. Kennedy MA, et al. ABCG1 has a critical role in mediating cholesterol efflux to HDL and preventing cellular lipid accumulation. *Cell Metabolism*. 2005;1(2):121–131.
20. Wang Z, Thurmond DC. Mechanisms of biphasic insulin-granule exocytosis – roles of the cytoskeleton, small GTPases and SNARE proteins. *J Cell Sci*. 2009;122(pt 7):893–903.
21. Evans-Molina C, et al. Peroxisome proliferator-activated receptor gamma activation restores islet function in diabetic mice through reduction of endoplasmic reticulum stress and maintenance of euchromatin structure. *Mol Cell Biol*. 2009;29(8):2053–2067.
22. Gustavsson N, et al. Impaired insulin secretion and glucose intolerance in synaptotagmin-7 null mutant mice. *Proc Natl Acad Sci U S A*. 2008;105(10):3992–3997.
23. Speidel D, et al. CAPS1 and CAPS2 regulate stability and recruitment of insulin granules in mouse pancreatic [beta] cells. *Cell Metabolism*. 2008;7(1):57–67.
24. Buchmann J, et al. Ablation of the cholesterol transporter adenosine triphosphate-binding cassette transporter G1 reduces adipose cell size and protects against diet-induced obesity. *Endocrinology*. 2007;148(4):1561–1573.
25. Klumperman J, Kuliawat R, Griffith JM, Geuze HJ, Arvan P. Mannose 6-phosphate receptors are sorted from immature secretory granules via adaptor protein AP-1, clathrin, and syntaxin 6-positive vesicles. *J Cell Biol*. 1998;141(2):359–371.
26. Eaton BA, Haugwitz M, Lau D, Moore HP. Biogenesis of regulated exocytotic carriers in neuroendocrine cells. *J Neurosci*. 2000;20(19):7334–7344.
27. Castle A, Castle D. Ubiquitously expressed secretory carrier membrane proteins (SCAMPs) 1-4 mark different pathways and exhibit limited constitutive trafficking to and from the cell surface. *J Cell Sci*. 2005;118(pt 16):3769–3780.
28. Liu L, Guo Z, Tieu Q, Castle A, Castle D. Role of secretory carrier membrane protein SCAMP2 in granule exocytosis. *Mol Biol Cell*. 2002; 13(12):4266–4278.
29. Kowluru A, Metz SA. Stimulation by prostaglandin E2 of a high-affinity GTPase in the secretory granules of normal rat and human pancreatic islets. *Biochem J*. 1994;297(pt 2):399–406.
30. Kim T, Gondre-Lewis MC, Arnaoutova I, Loh YP. Dense-core secretory granule biogenesis. *Physiology (Bethesda)*. 2006;21:124–133.
31. Dhanvantari S, Loh YP. Lipid raft association of carboxypeptidase E is necessary for its function as a regulated secretory pathway sorting receptor. *J Biol Chem*. 2000;275(38):29887–29893.
32. Wang Y, Thiele C, Huttner WB. Cholesterol is required for the formation of regulated and constitutive secretory vesicles from the trans-Golgi network. *Traffic*. 2000;1(12):952–962.
33. Churchward MA, Rogasevskaia T, Hofgen J, Bau J, Coorssen JR. Cholesterol facilitates the native mechanism of Ca2+-triggered membrane fusion. *J Cell Sci*. 2005;118(pt 20):4833–4848.
34. Gondre-Lewis MC, et al. Abnormal sterols in cholesterol-deficiency diseases cause secretory granule malformation and decreased membrane curvature. *J Cell Sci*. 2006;119(pt 9):1876–1885.
35. Yancey PG, et al. Cellular cholesterol efflux mediated by cyclodextrins. Demonstration Of kinetic pools and mechanism of efflux. *J Biol Chem*. 1996;271(27):16026–16034.
36. Hao M, Lin SX, Karylowski OJ, Wustner D, McGraw TE, Maxfield FR. Vesicular and non-vesicular sterol transport in living cells. The endocytic recycling compartment is a major sterol storage organelle. *J Biol Chem*. 2002;277(1):609–617.
37. Lange Y, Ye J, Steck TL. How cholesterol homeostasis is regulated by plasma membrane cholesterol in excess of phospholipids. *Proc Natl Acad Sci U S A*. 2004;101(32):11664–11667.
38. Gastaldelli A, Ferrannini E, Miyazaki Y, Matsuda M, Mari A, Defronzo RA. Thiazolidinediones improve beta-cell function in type 2 diabetic patients. *Am J Physiol Endocrinol Metab*. 2007;292(3):E871–E883.
39. Diani AR, Sawada G, Wyse B, Murray FT, Khan M. Pioglitazone preserves pancreatic islet structure and insulin secretory function in three murine models of type 2 diabetes. *Am J Physiol Endocrinol Metab*. 2004;286(1):E116–E122.
40. Gerin I, et al. LXR{beta} is required for adipocyte growth, glucose homeostasis, and {beta} cell function. *J Biol Chem*. 2005;280(24):23024–23031.
41. von Zastrow M, Castle JD. Protein sorting among two distinct export pathways occurs from the content of maturing exocrine storage granules. *J Cell Biol*. 1987;105(6 pt 1):2675–2684.
42. Ohara-Imaizumi M, Nishiwaki C, Kikuta T, Kumakura K, Nakamichi Y, Nagamatsu S. Site of docking and fusion of insulin secretory granules in live MIN6 beta cells analyzed by TAT-conjugated anti-syntaxin 1 antibody and total internal reflection fluorescence microscopy. *J Biol Chem*. 2004;279(9):8403–8408.
43. Grabner CP, Price SD, Lysakowski A, Cahill AL, Fox AP. Regulation of large dense-core vesicle volume and neurotransmitter content mediated by adaptor protein 3. *Proc Natl Acad Sci U S A*. 2006; 103(26):10035–10040.
44. Vaughan AM, Oram JF. ABCG1 redistributes cell cholesterol to domains removable by high density lipoprotein but not by lipid-depleted apolipoproteins. *J Biol Chem*. 2005;280(34):30150–30157.
45. Mondal M, Mesmin B, Mukherjee S, Maxfield FR. Sterols are mainly in the cytoplasmic leaflet of the plasma membrane and the endocytic recycling compartment in CHO cells. *Mol Biol Cell*. 2009;20(2):581–588.
46. Dean M, Hamon Y, Chimini G. The human ATP-binding cassette (ABC) transporter superfamily. *J Lipid Res*. 2001;42(7):1007–1017.
47. Kelly A, et al. Assembly and function of the two ABC transporter proteins encoded in the human major histocompatibility complex. *Nature*. 1992;355(6361):641–644.
48. Mackenzie SM, Howells AJ, Cox GB, Ewart GD. Sub-cellular localisation of the white/scarlet ABC transporter to pigment granule membranes within the compound eye of Drosophila melanogaster. *Genetica*. 2000;108(3):239–252.
49. Sato T, Herman L. Stereological analysis of normal rabbit pancreatic islets. *Am J Anat*. 1981;161(1):71–84.
50. Westhead EW. Lipid composition and orientation in secretory vesicles. *Ann N Y Acad Sci*. 1987;493:92–100.
51. Lange Y, Swaisgood MH, Ramos BV, Steck TL. Plasma membranes contain half the phospholipid and 90% of the cholesterol and sphingomyelin in cultured human fibroblasts. *J Biol Chem*. 1989;264(7):3786–3793.
52. Torra IP, et al. Phosphorylation of liver X receptor alpha selectively regulates target gene expression in macrophages. *Mol Cell Biol*. 2008;28(8):2626–2636.
53. Chen M, Bradley MN, Beaven SW, Tontonoz P. Phosphorylation of the liver X receptors. *FEBS Lett*. 2006;580(20):4835–4841.
54. Kaneto H, Xu G, Fujii N, Kim S, Bonner-Weir S, Weir GC. Involvement of c-Jun N-terminal kinase in oxidative stress-mediated suppression of insulin gene expression. *J Biol Chem*. 2002;277(33):30010–30018.
55. Harmon JS, Stein R, Robertson RP. Oxidative stress-mediated, post-translational loss of MafA protein as a contributing mechanism to loss of insulin gene expression in glucotoxic beta cells. *J Biol Chem*. 2005;280(12):11107–11113.
56. Bensinger SJ, et al. LXR signaling couples sterol metabolism to proliferation in the acquired immune response. *Cell*. 2008;134(1):97–111.
57. Nissen SE, Wolski K. Effect of rosiglitazone on the risk of myocardial infarction and death from cardiovascular causes. *N Engl J Med*.

2007;356(24):2457–2471.
58. Baldan A, et al. Impaired development of atherosclerosis in hyperlipidemic Ldlr$^{-/-}$ and ApoE$^{-/-}$ mice transplanted with Abcg1$^{-/-}$ bone marrow. *Arterioscler Thromb Vasc Biol*. 2006;26(10):2301–2307.
59. Yvan-Charvet L, et al. Combined deficiency of ABCA1 and ABCG1 promotes foam cell accumulation and accelerates atherosclerosis in mice. *J Clin Invest*. 2007;117(12):3900–3908.
60. Guest PC, Rhodes CJ, Hutton JC. Regulation of the biosynthesis of insulin-secretory-granule proteins. Co-ordinate translational control is exerted on some, but not all, granule matrix constituents. *Biochem J*. 1989;257(2):431–437.
61. Liu L, et al. SCAMP2 interacts with Arf6 and phospholipase D1 and links their function to exocytotic fusion pore formation in PC12 cells. *Mol Biol Cell*. 2005;16(10):4463–4472.
62. Yang Z, et al. Combined treatment with lisofylline and exendin-4 reverses autoimmune diabetes. *Biochem Biophys Res Commun*. 2006;344(3):1017–1022.
63. Nunemaker CS, et al. Individual mice can be distinguished by the period of their islet calcium oscillations: is there an intrinsic islet period that is imprinted in vivo? *Diabetes*. 2005;54(12):3517–3522.
64. Lee JY, et al. Prebeta high density lipoprotein has two metabolic fates in human apolipoprotein A-I transgenic mice. *J Lipid Res*. 2004;45(4):716–728.
65. Bligh EG, Dyer WJ. A rapid method of total lipid extraction and purification. *Can J Biochem Physiol*. 1959;37(8):911–917.
66. Chen PS, Toribara TY, Warner H. Microdetermination of phosphorus. *Anal Chem*. 1956;28(11):1756–1758.
67. Rudel LL, Kelley K, Sawyer JK, Shah R, Wilson MD. Dietary monounsaturated fatty acids promote aortic atherosclerosis in LDL Receptor–Null, human ApoB100–Overexpressing transgenic mice. *Arterioscler Thromb Vasc Biol*. 1998;18(11):1818–1827.
68. Nevins AK, Thurmond DC. A direct interaction between Cdc42 and vesicle-associated membrane protein 2 regulates SNARE-dependent insulin exocytosis. *J Biol Chem*. 2005;280(3):1944–1952.
69. Stinchcombe JC, Huttner WB. Purification of secretory granules from PC12 cells. In: Celis JE, ed. *Cell Biology, A Laboratory Handbook*. San Diego, CA: Academic Press; 1994:557–566.
70. Bolte S, Cordelieres FP. A guided tour into subcellular colocalization analysis in light microscopy. *J Microsc*. 2006;224(pt 3):213–232.
71. Weixel K, Bradbury NA. Analysis of CFTR endocytosis by cell surface biotinylation. *Methods Mol Med*. 2002;70:323–340.
72. Armstrong AJ, Gebre AK, Parks JS, Hedrick CC. ATP-binding cassette transporter G1 negatively regulates thymocyte and peripheral lymphocyte proliferation. *J Immunol*. 2010;184(1):173–183.
73. Guo Z, Liu L, Cafiso D, Castle D. Perturbation of a very late step of regulated exocytosis by a secretory carrier membrane protein (SCAMP2)-derived peptide. *J Biol Chem*. 2002;277(38):35357–35363.